

Samuel Luiz Pinheiro Gonçalves Beres

**$B_c, B_c^*, B_s, B_s^*, D_s$  and  $D_s^*$  mass shift  
in a nuclear medium**

arXiv:2407.03377v2 [hep-ph] 24 Jul 2024

São Paulo, Março de 2024

UNIVERSIDADE CIDADE DE SÃO PAULO  
PROGRAMA DE PÓS-GRADUAÇÃO  
EM ASTROFÍSICA E FÍSICA COMPUTACIONAL

Samuel Luiz Pinheiro Gonçalves Beres

**$B_c, B_c^*, B_s, B_s^*, D_s$  and  $D_s^*$  mass shift  
in a nuclear medium**

São Paulo, Março de 2024

**Samuel Luiz Pinheiro Gonçalves Beres**

**$B_c, B_c^*, B_s, B_s^*, D_s$  and  $D_s^*$  mass shift  
in a nuclear medium**

Texto apresentado ao Programa de Pós-Graduação em Astrofísica e Física Computacional da Universidade Cidade de São Paulo, para defesa do Mestrado, sob a orientação do Dr. Kazuo Tsushima.

São Paulo, Março de 2024.

## Sistema de Bibliotecas do Grupo Cruzeiro do Sul Educacional

B491b Beres, Samuel Luiz Pinheiro Gonçalves.  
Bc, B\*c, Bs, B\*s, Ds and D\*s mass shift in a nuclear  
medium./ Samuel Luiz Pinheiro Gonçalves Beres. - São  
Paulo: Universidade Cidade de São Paulo, 2024.  
61 f.: il.

Dissertação (Mestrado) – Universidade Cidade de São  
Paulo, Programa de Pós Graduação em Astrofísica e Física  
Computacional, 2024.

Orientador: Prof Dr. Kazuo Tsushima

1. Meio nuclear. 2. Mudança de massa. 3. Física de  
partículas. 4. Cromodinâmica quântica (QCD). I. Tsushima,  
Kazuo, orient. II. Título.

CDD 523.01

Samuel Luiz Pinheiro Gonçalves Beres

**$B_c, B_c^*, B_s, B_s^*, D_s$  and  $D_s^*$  mass shift  
in a nuclear medium**

Texto apresentado ao Programa de Pós-Graduação em Astrofísica e Física Computacional da Universidade Cidade de São Paulo, para defesa do Mestrado, sob a orientação do Dr. Kazuo Tsushima.

Aprovada em Março de 2024.

BANCA EXAMINADORA

---

Prof. Dr. Kazuo Tsushima - Orientador  
UNIVERSIDADE CIDADE DE SÃO PAULO

---

Prof. Dr. João Pacheco B. C. de Melo  
UNIVERSIDADE CIDADE DE SÃO PAULO

---

Prof. Dr. Gastão I. Krein  
UNIVERSIDADE ESTADUAL DE SÃO PAULO

São Paulo, Março de 2024

To my Aunt and my friend Danilo for all the support and incentives in times of storm. To my supervisor Dr. Kazuo Tsushima, my inspiration and definition of excellence in work and research, thank you for taught me to continuously improve.

## Acknowledgements

My thanks go to Professor Kazuo Tsushima for being so patient and for all the lessons and advice that allowed me to grow as a student and better person, for all that I will be forever grateful.

Thanks go to my senior colleague Ms. Guilherme N. Zeminiani and all my dear colleagues and professors of LFTC. I would like to thank especially Professor Gastão I. Krein of Universidade Estadual de São Paulo (UNESP) and Professor Fernando S. Navarra of Universidade de São Paulo (USP) for their kindness to be the committee members of the thesis/master defense of mine.

Finally thanks to Universidade Cidade de São Paulo and Dr. Gustavo A. Lanfranchi for the support and opportunity.

This study was financed in part by the Coordenação de Aperfeiçoamento de Pessoal de Nível Superior – Brasil (CAPES) – Finance Code 001.

*“If I have seen further than others, it is by standing upon the shoulders of giants.”*

*Isaac Newton*

# List of Figures

2.1	$B$ and $B^*$ (left panel), $D$ and $D^*$ (middle panel) and $K$ and $K^*$ (right panel) meson Lorentz-scalar effective masses in symmetric nuclear matter versus baryon density ( $\rho_B/\rho_0$ ), calculated by the QMC model. . . . .	13
2.2	The lowest one-loop order self-energy of particle $A$ . From the left- to right-direction we have an incoming particle $A$ carrying a momentum ( $p$ ) which will reach the vertex and dissociate into two virtual particles denoted by $B$ and $C$ carrying a respective momentum $k_1$ and $k_2$ and finally recombine into $A$ again. . . . .	14
2.3	Pseudoscalar meson self-energies in two lighter meson excitations in the one-loop order, for $B_c$ (top panel), $B_s$ (middle panel), and $D_s$ (bottom panel). . . . .	15
2.4	Vector meson self-energies for $B_c^*$ (top panel), $B_s^*$ (middle panel) and $D_s^*$ (bottom panel) in the lowest order. . . . .	15
3.1	In-medium mass (left panel) and mass shift (right panel) of $B_c$ meson (i) only including the $B^*D$ loop (top) and (ii) only including the $BD^*$ . $\rho_0 = 0.15 fm^{-3}$ is the symmetric nuclear matter saturation density and $\rho_B$ is the baryon density. . . . .	29
3.2	$B_c$ self-energy values considering total two possible loops. Each figure shows the self-energy for total loop considering both loops for a different cutoff value. $\rho_0 = 0.15 fm^{-3}$ is the symmetric nuclear matter saturation density and $\rho_B$ is the baryon density. . . . .	30
3.3	Decomposition of the $B_c$ meson total self-energy for different cutoff mass values. . . . .	32
3.4	$B_c$ in-medium mass (left) and mas shift (right). $\rho_0 = 0.15 fm^{-3}$ is the symmetric nuclear matter saturation density and $\rho_B$ is the baryon density. . . . .	32

3.5	$B_c^*$ self-energies for different cutoff mass values. . . . .	33
3.6	$B_c^*$ in-medium mass (left) and mas shift (right). $\rho_0 = 0.15 \text{ fm}^{-3}$ is the symmetric nuclear matter saturation density and $\rho_B$ is the baryon density. . . . .	33
3.7	In-medium mass (left panel) and mass shift (right panel) of $B_s^0$ meson (i) only including the $BK^*$ loop (top) and (ii) only including the $B^*K$ . $\rho_0 = 0.15 \text{ fm}^{-3}$ is the symmetric nuclear matter saturation density and $\rho_B$ is the baryon density. . . . .	34
3.8	$B_s^0$ self-energy values. Each panel shows the self-energy for total loop contribution including the both loops but for a different cutoff value. The figure in the bottom-right panel shows a comparison among all of them including the total and the two possible loops separately. . . . .	35
3.9	$B_s^0$ in-medium mass (left) and mas shift (right). $\rho_0 = 0.15 \text{ fm}^{-3}$ is the symmetric nuclear matter saturation density and $\rho_B$ is the baryon density. . . . .	36
3.10	$B_s^*$ self-energies for different cutoff mass values. . . . .	37
3.11	$B_s^*$ in-medium mass (left) and mass shift (right). . . . .	38
3.12	In-medium mass (left panel) and mass shift (right panel) of $D_s$ meson (i) only including the $D^*K$ loop (top) and (ii) only including the $DK^*$ . $\rho_0 = 0.15 \text{ fm}^{-3}$ is the symmetric nuclear matter saturation density and $\rho_B$ is the baryon density. . . . .	39
3.13	$D_s$ self-energy values. Each panel shows the self-energy for the total loop contribution from both loops but a different cutoff value, and the figure in the right-bottom panel shows a comparison among all of them including the total and two different each possible loop. . . . .	40
3.14	$D_s$ in-medium mass (left) and mas shift (right). $\rho_0 = 0.15 \text{ fm}^{-3}$ is the symmetric nuclear matter saturation density and $\rho_B$ is the baryon density. . . . .	41
3.15	$D_s^*$ self-energies for different cutoff mass values. . . . .	42
3.16	$D_s^*$ in-medium mass (left) and mass shift (right). . . . .	42
4.1	Comparison of the in medium mass shift of pseudoscalar (top) and vector (bottom) mesons, $\eta_b$ (top-left), $B_c$ (top-center) $\eta_c$ (top-right) $\Upsilon$ (bottom-left), $B_c^*$ (bottom-center) and $J/\Psi$ (bottom-right). $\rho_0 = 0.15 \text{ fm}^{-3}$ is the symmetric nuclear matter saturation density and $\rho_B$ is the baryon density. . . . .	45

6.1 Integration of  $\kappa_0$  in the complex plane. . . . . 48

8.1 VDM feynman diagram . . . . . 55

# List of Tables

1.1	Lepton properties. In the third column entry, $ e $ is the absolute value of the electron charge. $[L_e, L_\mu, L_\tau]$ is respectively the $[e$ (electron), $\mu$ (muon), $\tau$ (tauon)] (lepton) number. The lepton number is 1 for all the leptons, $-1$ for all the antileptons, and 0 for non-leptons. . . . .	2
1.2	Quark properties. $I_z$ is the third component of the quark isospin, (being given by the $(1/2)\tau_z$ , the Pauli matrix divided by 2), and all other quarks except u and d have $I_z=0$ . . . . .	3
1.3	Boson properties. . . . .	3
1.4	Some typical low mass baryons and their quark components [11]. . . . .	4
1.5	Table of Mesons. . . . .	5
1.6	Density dependence of meson (effective) masses in MeV calculate in the QMC model with $m_{u,d} = 5$ MeV, $m_s = 250$ MeV, $m_c = 1270$ MeV and $m_b = 4200$ MeV. (See Ref. [40].) ( $\rho_0 = 0.15$ fm $^{-3}$ below.) Mass is independent of the charge states when we ignore the isospin symmetry breaking like below. Note that, for the $m_{B_c^*}$ value we take the average value in Ref. [50]. . . . .	8
3.1	$\Delta m$ for $B_c$ meson at $3\rho_0$ for all the five cutoff value ( $\Lambda = 2000, 3000, 4000, 5000, 6000$ MeV). . . . .	31
3.2	$m^0$ considering $B^*D$ loop, $BD^*$ loop and total $B^*D + BD^*$ . . . . .	31
3.3	$\Delta m$ in medium for $B_c^*$ meson at $3\rho_0$ for all the five cutoff value ( $\Lambda = 2000, 3000, 4000, 5000, 6000$ MeV). . . . .	31
3.4	$m^0$ considering $BD$ loop. . . . .	34
3.5	$\Delta m$ in medium for $B_s^0$ meson at $3\rho_0$ for all the five cutoff value ( $\Lambda = 2000, 3000, 4000, 5000, 6000$ MeV). . . . .	36
3.6	$m^0$ considering $B^*K$ loop $BK^*$ loop and total $B^*K + BK^*$ . . . . .	37

3.7	$\Delta m$ in medium for $B_s^*$ meson at $3\rho_0$ for all the five cutoff value ( $\Lambda = 2000, 3000, 4000, 5000, 6000$ MeV). . . . .	38
3.8	$m^0$ considering $BK$ loop. . . . .	38
3.9	$\Delta m$ for $D_s$ meson at $3\rho_0$ for all the five cutoff value ( $\Lambda = 2000, 3000, 4000, 5000, 6000$ MeV). . . . .	39
3.10	$m^0$ considering $D^*K$ loop $DK^*$ loop and total $D^*K + DK^*$ . . . . .	41
3.11	$\Delta m$ for $D_s^*$ meson at $3\rho_0$ for all the five cutoff value ( $\Lambda = 2000, 3000, 4000, 5000, 6000$ MeV). . . . .	41
3.12	$m^0$ considering $DK$ loop. . . . .	43
3.13	Density dependence of meson (effective) masses in MeV calculate in the QMC model with $m_{u,d} = 5$ MeV, $m_s = 250$ MeV, $m_c = 1270$ MeV and $m_b = 4200$ MeV. ( $\rho_0 = 0.15$ fm <sup>-3</sup> below.) . . . . .	43

# Contents

List of Figures . . . . .	x
Lista de Tabelas . . . . .	xii
<b>Resumo</b>	<b>xv</b>
<b>Abstract</b>	<b>xvi</b>
<b>1 Introduction</b>	<b>1</b>
1.1 Brief Summary of Particle Physics . . . . .	1
1.2 Motivations . . . . .	4
1.3 Why $B_c$ and $B_c^*$ ? . . . . .	8
<b>2 Meson Mass-Shift Calculation</b>	<b>11</b>
2.1 The Quark-Meson Coupling Model . . . . .	11
2.2 Meson Self-Energy . . . . .	14
2.3 Interaction Lagrangian . . . . .	16
2.4 Self-energy Calculation . . . . .	17
<b>3 Results</b>	<b>27</b>
3.1 $B_c$ and $B_c^*$ meson results . . . . .	27
3.2 $B_s^0$ and $B_s^*$ meson results . . . . .	34
3.3 $D_s$ and $D_s^*$ meson results . . . . .	37
<b>4 Comparison with heavy quarkonia</b>	<b>44</b>
<b>5 Conclusion</b>	<b>46</b>
<b>6 Appendix A</b>	<b>48</b>
6.1 Poles in integration . . . . .	48

<b>7 Appendix B</b>	<b>50</b>
7.1 SU(5) generators . . . . .	50
7.2 Adjoint Representation . . . . .	52
<b>8 Appendix C</b>	<b>54</b>
8.1 Coupling constant calculation . . . . .	54

# Resumo

Pela primeira vez, estimamos a mudança de massa dos mésons pesados de dois sabores  $B_c, B_c^*, B_s, B_s^*, D_s$  e  $D_s^*$  em matéria nuclear simétrica. As estimativas são feitas avaliando as autoenergias de um loop de ordem mais baixa. A origem dessas mudanças de massa são as mudanças nos mésons pesados e leves do estado intermediário dos mésons pesados de dois sabores em matéria nuclear simétrica. Nossos resultados mostram que a magnitude da mudança de massa para o méson  $B_c$  ( $\bar{b}c$  ou  $b\bar{c}$ ) é maior que a mudança de massa dos mésons  $\eta_c(\bar{c}c)$  e  $\eta_b(\bar{b}b)$ , diferente da expectativa de que seria o meio termo entre eles. Enquanto, o de  $B_c^*$  mostra o meio termo entre as de  $J/\psi$  e  $\Upsilon$ . Observamos que a excitação do méson vetorial mais leve nos loops dos mésons pseudoescalares, faz com que a autoenergia contribua mais para mudança de massa do méson correspondente,  $B_c, B_s$ , e  $D_s$ . (Os principais resultados dessa tese foram apresentados no artigo Ref. [1].)

**Palavras-chave:** meio nuclear, mudança de massa, física de partículas, cromodinâmica quântica (QCD), mésons pesados.

# Abstract

For the first time, we estimate the in-medium mass shift of the two-flavored heavy mesons  $B_c, B_c^*, B_s, B_s^*, D_s$  and  $D_s^*$  in symmetric nuclear matter. The estimates are made by evaluating the lowest order one-loop self-energies. The enhanced excitations of intermediate state heavy-light quark mesons in symmetric nuclear matter are the origin of their negative mass shift. Our results show that the magnitude of the mass shift for the  $B_c$  meson ( $\bar{b}c$  or  $b\bar{c}$ ) is larger than those of the  $\eta_c(\bar{c}c)$  and  $\eta_b(\bar{b}b)$ , different from a naive expectation that it would be in-between of them. While, that of the  $B_c^*$  shows the in-between of the  $J/\psi$  and  $\Upsilon$ . We observe that the lighter vector meson excitation in each meson self-energy gives a dominant contribution for the corresponding meson mass shift,  $B_c, B_s$ , and  $D_s$ . (Main results of this thesis are presented in the article Ref. [1].)

**Keywords:** nuclear medium, mass-shift, particle physics, quantum chromodynamics (QCD), heavy mesons.

# Chapter 1

## Introduction

### 1.1 Brief Summary of Particle Physics

The study of "what matter is made of" began many centuries ago in Ancient Greece. Many philosophers tried to answer this question, namely, to find the arché, the elements from where (supposedly) everything comes from. For example, Anaximenes proposed that all forms of matter can be obtained by condensing or rarefying air [2]. In 19th century, John Dalton, concluded that each element was composed by atoms. But, in 20th century with the development of quantum physics (atomic, nuclear and elementary particle physics), in particular during the years 1950s and 1960s, many subatomic particles were found in collisions of particles by high energy beams [3, 4, 5, 20]. Based on the huge amount of accumulated experimental data, human beings have established a theory of elementary particles and their interactions, the Standard Model (SM) [6, 7]

The elementary particles, we mean by this the building blocks of the Standard Model (SM), fermions particularly, leptons (see Table 1.1) and quarks (see Table 1.2), and bosons (see Table 1.3) [8], where the quarks compose the ordinary matter. Leptons interact electromagnetically and weakly, but only weakly if they are not charged, while quarks interact via all three interactions, weak, strong and electromagnetic. We may consider gravitational interaction at the elementary particle level, but the strength of the gravitational force is approximately  $10^{-36}$  times of that of the electromagnetic force,  $10^{-29}$  times of that of the weak force, and  $10^{-38}$  times of that of the strong force (100 trillions trillions trillions times weaker). Thus, we can ignore the gravitational interaction in the following, because the strength is irrelevant for the elementary particles in SM.

Lepton	Mass (MeV)	Charge (in units of $ e $ )	$L_e$	$L_\mu$	$L_\tau$
$e^-$	0.510	-1	1	0	0
$\mu^-$	105.6	-1	0	1	0
$\tau^-$	1776	-1	0	0	1
$\nu_e$	$< 2.2 \times 10^{-5}$	0	1	0	0
$\nu_\mu$	$< 0.17$	0	0	1	0
$\nu_\tau$	$< 15.5$	0	0	0	1

Table 1.1: Lepton properties. In the third column entry,  $|e|$  is the absolute value of the electron charge.  $[L_e, L_\mu, L_\tau]$  is respectively the [ $e$  (electron),  $\mu$  (muon),  $\tau$  (tauon)] (lepton) number. The lepton number is 1 for all the leptons,  $-1$  for all the antileptons, and 0 for non-leptons.

Hadrons, the strong-interaction particles (bound states of quarks and/or anti-quarks), have mostly two kinds, baryons that are composed of three quarks, mesons that are composed of a pair of quark and antiquark. There have also been found and established the existence for exotic matter called tetra-quark [9], the strong-interaction bound system composed of two quarks and two antiquarks, and pentaquark [9], the strong-interaction bound system composed of four quarks and one antiquark. All such observed particles are realized as the "color-singlet" states dictated by the color gauge theory of quantum chromodynamics (QCD).

Quantum chromodynamics, is accepted as the theory of the strong interaction among quarks and gluons [10], that is to say, the interactions between and among hadrons. As examples, we list the low mass baryons and mesons in Tables 1.4 and 1.5 (see Ref. [11]), respectively.

Quarks ( $q$ ) have six "flavors" up ( $u$ ), down ( $d$ ), strange ( $s$ ), charm ( $c$ ), bottom ( $b$ ) and top ( $t$ ). But they can only be deduced to exist in nature as bound systems with two or more quarks forming a baryon ( $qqq$ ) or with an antiquark forming a meson ( $q\bar{q}$ ). Some exotic states were also found, like tetraquark ( $qq\bar{q}\bar{q}$ ) and pentaquark ( $qqq\bar{q}\bar{q}$ ) [12]. In QCD, all of such particles form "color singlet states", particularly only the color singlet states can be observed. Equivalently, since all individual quarks have "a color quantum number", no isolated quarks can be, or have been found, and this fact is called "confinement" in QCD of strong interaction in SM.

Flavor	Mass (MeV)	Charge (in units of $ e $ )	Properties
u	2	$\frac{2}{3}$	$I_z = \frac{1}{2}$
d	5	$-\frac{1}{3}$	$I_z = -\frac{1}{2}$
s	100	$-\frac{1}{3}$	Strangeness = -1
c	1200	$\frac{2}{3}$	Charm = +1
b	4200	$-\frac{1}{3}$	Bottom = -1
t	174000	$\frac{2}{3}$	Top = +1

Table 1.2: Quark properties.  $I_z$  is the third component of the quark isospin, (being given by the  $(1/2)\tau_z$ , the Pauli matrix divided by 2), and all other quarks except u and d have  $I_z=0$ .

Boson	Mass (GeV)	Spin	Force
Gluon $g$	0	1	strong
Photon $\gamma$	0	1	electromagnetic
W-boson $W^\pm$	80.4	1	weak
Z-boson $Z^0$	91.2	1	weak
Higgs-boson $H$	126	0	gravitation

Table 1.3: Boson properties.

Although baryons and mesons are both hadrons, baryons follow the Fermi-Dirac statistics (fermions), and have half-integer spins ( $\frac{1}{2}, \frac{3}{2}, \dots$ ), while the mesons follow the Bose-Einstein statistics, and have zero or integer spins (0,1,2...).

To explain the existence of baryons, for example  $\Delta^{++}$  [13] in nature as experimentally observed without contradicting the Pauli exclusion principle, as well as to explain the  $\pi^0 \rightarrow \gamma\gamma$  decay rate correctly [14], the "color charge" was introduced (one of the basics of QCD).

Spin and Parity can conveniently classify mesons: vector meson (total spin = 1 and odd parity), pseudovector (axial-vector) meson (total spin = 1 and even parity), scalar meson (total spin = 0 and even parity), pseudoscalar meson (total spin = 0 and odd parity). Also other higher spin mesons exist (spin 2) and have been found, such as tensor mesons, etc. While for baryons, although such easier classification does not exist, the

Name	Particle label	Quark Component	Rest Mass (MeV)	Spin
Proton	p	uud	938.3	$\frac{1}{2}$
Neutron	n	ddu	939.6	$\frac{1}{2}$
Lambda	$\Lambda^0$	uds	1115.6	$\frac{1}{2}$
Sigma	$\Sigma^+$	uus	1189.4	$\frac{1}{2}$
Sigma	$\Sigma^0$	uds	1192.5	$\frac{1}{2}$
Sigma	$\Sigma^-$	dds	1197.3	$\frac{1}{2}$
Delta	$\Delta^{++}$	uuu	1232	$\frac{3}{2}$
Delta	$\Delta^+$	uud	1232	$\frac{3}{2}$
Delta	$\Delta^0$	udd	1232	$\frac{3}{2}$
Delta	$\Delta^-$	ddd	1232	$\frac{3}{2}$
Xi	$\Xi^0$	uss	1315	$\frac{1}{2}$
Xi	$\Xi^-$	dss	1321	$\frac{1}{2}$
Omega	$\Omega^-$	sss	1672	$\frac{3}{2}$
Lambda	$\Lambda_c^+$	udc	2281	$\frac{1}{2}$

Table 1.4: Some typical low mass baryons and their quark components [11].

nucleon resonances have been found up to spin  $13/2$ , and those of the  $\Delta$  up to spin  $15/2$ . (See Ref. [11].)

## 1.2 Motivations

In particle and nuclear physics, nuclear matter is a kind of idealistically considered infinitely large system, that consists of many nucleons (usually zero-temperature is assumed). Specifically, it may be regarded as (partly) correspond to the environment inside the central region of a heavy nucleus where nucleons (protons and neutrons) interact each other through the strong force. In particular, symmetric nuclear matter is a system of uniform, isospin and spin saturated infinitely large system, and (usually) zero temperature with equal number of protons and neutrons.

Inside atomic nuclei, protons and neutrons are bound together by the strong force. At low energies and finite baryon densities, the nuclear medium can significantly affect the properties of nucleons, e.g., modifying their effective masses, interactions, and other

Name	Particle label	Antiparticle label	Quark Component	Rest Mass (MeV)	Spin
Pion	$\pi^+$	$\pi^-$	$u\bar{d}$	139.6	0
Pion	$\pi^0$	$\pi^0$	$\frac{u\bar{u}-d\bar{d}}{\sqrt{2}}$	135.0	0
Kaon	$K^+$	$K^-$	$u\bar{s}$	493.7	0
Kaon	$K_s^0$	$\bar{K}_s^0$	$\frac{d\bar{s}+s\bar{d}}{\sqrt{2}}$	497.6	0
Kaon	$K_L^0$	$\bar{K}_L^0$	$\frac{d\bar{s}-s\bar{d}}{\sqrt{2}}$	497.6	0
Eta	$\eta^0$	$\eta^0$	$\frac{u\bar{u}+d\bar{d}-2s\bar{s}}{\sqrt{6}}$	547.9	0
Eta prime	$\eta'^0$	$\eta'^0$	$\frac{u\bar{u}+d\bar{d}+s\bar{s}}{\sqrt{3}}$	958	0
Rho	$\rho^+$	$\rho^-$	$u\bar{d}$	770	1
Rho	$\rho^0$	$\rho^0$	$\frac{u\bar{u}-d\bar{d}}{\sqrt{2}}$	770	1
Omega	$\omega^0$	$\omega^0$	$\frac{u\bar{u}+d\bar{d}}{\sqrt{2}}$	782	1
Phi	$\phi^0$	$\phi^0$	$s\bar{s}$	1020	1
D-meson	$D^+$	$D^-$	$c\bar{d}$	1869.7	0
D-meson	$D^0$	$\bar{D}^0$	$c\bar{u}$	1864.8	0
D <sub>s</sub> -meson	$D_s^+$	$D_s^-$	$c\bar{s}$	1968.3	0
J/Psi	$J/\psi$	$J/\psi$	$c\bar{c}$	3096.9	1
B-meson	$B^-$	$B^+$	$b\bar{u}$	5279.3	0
B-meson	$B^0$	$\bar{B}^0$	$d\bar{b}$	5279.7	0
B <sub>s</sub> -meson	$B_s^0$	$\bar{B}_s^0$	$s\bar{b}$	5366.9	0
B <sub>c</sub> -meson	$B_c^+$	$B_c^-$	$c\bar{b}$	6274.5	0
Upsilon	$\Upsilon$	$\Upsilon$	$b\bar{b}$	9460.4	1

Table 1.5: Table of Mesons.

properties compared to those in free-space [15]. Thus, generally hadron properties are also expected be modified by the effects of surrounding nuclear medium when they are immersed in the nuclear medium [16, 17, 18].

During the last decades, many scientists have tried to study the effects of nuclear medium using various different approaches. A lot of experimenters use large accelerators for colliding particles with extremely high velocities/energies to investigate the structure of hadrons, and the production of short-lived forms of matter.

At modern major experimental facilities in the world, such as JLab (Thomas Jef-

fermion Accelerator Facilities, USA), RHIC (Relativistic Heavy Ion Collider, USA), Fermi Lab (Fermi National Accelerator Laboratory, USA), BNL (Brookhaven National Laboratory, USA), J-PARC (Japan Proton Accelerator Research Complex), SPring-8 (Super Photon Ring - 8 GeV), DESY (Deutsches Elektronen-Synchrotron, Germany), FAIR (Facility for Antiproton and Ion Research, Germany), COSY (Cooler Synchrotron), CERN (Conseil européen pour la recherche nucléaire, France), and BES III (Beijing Spectrometer III, China), huge number of experiments are going on and have been planned to study the properties of hadrons [19, 20] in free space as well as in a nuclear medium.

As mentioned before, each meson is a particle composed of a bound quark-antiquark pair [21]. When mesons are placed in a strongly interacting medium, such as dense nuclear environment, properties of mesons are expected to be modified due to the interactions with the surrounding particles (nucleons = protons and neutrons) and generated fields in the medium [22].

The dissociation [23] and regeneration of mesons can occur in extreme conditions, such as in a quark-gluon plasma (QGP) formed in high-energy heavy-ion collisions [24]. In this QGP phase, the temperature and density are so high that quarks and gluons are no longer confined within hadrons [25], and the mesons can dissociate into their constituents, quarks and antiquarks [26]. Meson regeneration can occur in QGP, i.e., the process by which mesons are recreated within the QGP medium. However, recall that, according to QCD, we cannot directly observe the QGP medium or isolated quarks.

The width of a meson, which is associated with the possible meson decay and other hadron creation channels, can be modified from its free space when it is in medium, because of the interactions [27]. Often it is referred to as width broadening, and it can provide insights into the scattering and absorption processes involving mesons.

In a nuclear medium, mesons can couple to different mesons and baryons with different spins and isospins. The interactions between meson and the surrounding nuclear medium can generate very interesting phenomena, in particular, a formation of meson-nucleus bound states.

A meson-nucleus bound state is an exotic state which a meson is bound in a nucleus by the attractive strong interaction (potential) between the meson and the nucleus [28].

One of the most prominent such in-medium modifications may be the change in the "effective" mass of mesons. In free space, mesons have well-defined observed physical

masses. However, in a nuclear medium, the interactions between mesons and nucleons can lead to shift in their Lorentz scalar "masses", or can add Lorentz scalar potentials [29]. This phenomena that we referred to as "mass shift" of mesons in a medium, is consequences of strong interactions of mesons and surrounding nuclear medium. This is probably one of the most interesting topics in nuclear and hadron physics. This "mass shift", in particular, of two-flavored heavy mesons, is the main subject of this thesis.

With many attempts to find the evidence and understand the origin of hadron masses and mass shift, it is clear that one has to study and understand well their properties/masses in free space. Hadron property change in medium has been extensively studied through various theoretical and experimental approaches [30, 31, 32, 33, 34, 35, 36, 37].

In the presence of nuclear medium, mesons are expected to change their properties due to the strong and many-body interactions among the mesons and nucleons (hadrons). These interactions would lead to shift in energies (Lorentz vector) and Lorentz scalar properties, which, according to the mass-energy equivalence principle, result in "changes" in meson effective masses (mass shift).

This meson mass shift can be attributed to the partial restoration of chiral symmetry—restoration of spontaneous and/or dynamical chiral symmetry, since the negative mass shift is associated with the reduction in the magnitude of (light quark) quark condensate (the order parameter of chiral symmetry).

In the presence of a nuclear medium, this symmetry breaking pattern can be modified and would be realized as mass modifications of mesons [38, 39] (negative mass shift).

In table 1.6 we present the density dependence of some meson effective masses in MeV calculated in the quark-meson coupling (QMC) model [40]. We will explain later in detail how the "effective meson masses" for  $B_c, B_c^*, B_s, B_s^*, D_s$  and  $D_s^*$  in symmetric nuclear matter are calculated in Table 1.6.

The study of hadron properties in a nuclear medium is of fundamental to nuclear physics, which deals with the structure and behavior of atomic nuclei. This is crucial for understanding the strong force or QCD, which is responsible for binding the protons and neutrons together in the nucleus.

Thus, understanding the properties of nuclear matter is naturally important for various fields, even such as astrophysics and cosmology, since it plays a crucial role in the early universe, in tight connection with the structure of neutron star and compact star

Table 1.6: Density dependence of meson (effective) masses in MeV calculate in the QMC model with  $m_{u,d} = 5$  MeV,  $m_s = 250$  MeV,  $m_c = 1270$  MeV and  $m_b = 4200$  MeV. (See Ref. [40].) ( $\rho_0 = 0.15 \text{ fm}^{-3}$  below.) Mass is independent of the charge states when we ignore the isospin symmetry breaking like below. Note that, for the  $m_{B_c^*}$  value we take the average value in Ref. [50].

	$\rho_B = 0$	$\rho_B = \rho_0$	$\rho_B = 2\rho_0$	$\rho_B = 3\rho_0$
$m_K$	493.7	430.5	393.6	369.0
$m_{K^*}$	893.9	831.9	797.2	775.0
$m_D$	1867.2	1805.2	1770.6	1748.4
$m_{D^*}$	2008.6	1946.9	1912.9	1891.2
$m_B$	5279.3	5218.2	5185.1	5164.4
$m_{B^*}$	5324.7	5263.7	5230.7	5210.2
$m_{B_c}$	6274.5			
$m_{B_c^*}$	6333.0			
$m_{B_s}$	5366.9			
$m_{B_s^*}$	5415.4			
$m_{D_s}$	1968.4			
$m_{D_s^*}$	2112.2			

structure.

### 1.3 Why $B_c$ and $B_c^*$ ?

Among many particles found so far within the category of standard model (SM),  $B_c$  and  $B_c^*$  mesons can play special roles for studying the interactions between the heavy quarks and light quarks ( $u$  and  $d$ ), especially the two-flavored heavy meson ( $B_c$  or  $B_c^*$ ) interactions with the nuclear medium.

$B_c$  and  $B_c^*$  mesons are composed by two heavy flavors of quarks, bottom ( $b$ ) and charm ( $\bar{c}$ ), i.e.,  $b\bar{c}$  (or  $\bar{b}c$ ), making them invaluable in probing dynamics of the strong force within quantum chromodynamics (QCD) in the nuclear medium, since nuclear medium itself does not contain heavy quarks  $b$  ( $\bar{b}$ ) or  $c$  ( $\bar{c}$ ).

This fact, based on the OZI-rule [41, 42, 43], suppresses that interactions of  $B_c$  and  $B_c^*$  mesons with the light-flavored meson and light baryon exchanges in the lowest order, and the interactions should be dominated by the gluons. Thus, we have good chances to explore the roles of gluons for the interactions of these mesons and the nuclear medium.

This will provide us with the opportunity to compare the strengths of meson-(nuclear matter) interactions among quarkonia and two-heavy flavored mesons. Another interest is that, whether or not the naive expectation that the (bottom-charmed meson)-(nuclear matter) interaction strength is in-between those of the (charmonia-nuclear matter) and (bottomonia-nuclear matter).

The  $B_c$  meson (spin-0 pseudoscalar), first theoretically studied in the early 1980s, and subsequently observed experimentally in 1998 at Fermi National Accelerator Laboratory (Fermi Lab) [44], to have a relatively longer lifetime compared to other mesons. This, along with its unique quark composition, makes the  $B_c$  meson an ideal candidate for investigating its properties, in particular the interaction with the nuclear medium.  $B_c^*$  meson (spin-1 vector), an excited state of the  $B_c$  meson, can offer equally excellent opportunities for exploration. Specifically, the  $B_c$  and  $B_c^*$  mesons serve as sensitive probes for exploring CP violation, flavor physics, and the search for rare decays. Due to the fact that the  $B_c$  meson is composed of two heavy quarks with two different flavors  $b$  and  $c$ , it is naively expected to possess intermediate properties in both mass and size of quarkonia composed of  $(b\bar{b})$  and  $(c\bar{c})$ . Besides that, its ground state can not annihilate into gluons or photons, what provides a special role compared to the quarkonium to examine heavy quark properties.

Furthermore, we focus on the mesons  $B_s$  and  $B_s^*$  (composed of  $b\bar{s}$  and  $\bar{b}s$ ) as well  $D_s$  and  $D_s^*$  (composed of  $c\bar{s}$  and  $\bar{c}s$ ).

Since such two different non-light flavored meson ground states cannot annihilate into gluons or photons, they also play special roles compared to the quarkonia ( $c\bar{c}$  and  $b\bar{b}$  mesons).

By the project of the present thesis, therefore, we can deepen our understanding on the strong interactions focusing on the heavy quarks. Moreover, although indirectly, we can study the effect of partial restoration of chiral symmetry in a nuclear medium, by studying the self-energies of such two-heavy-quark-flavored mesons interacting with the nuclear medium via the excitations of mesons with heavy-light quarks in the intermediate

states [45, 46, 47, 48, 49].

Recently, studies on the properties  $B_c$  and  $B_c^*$  (indeed, the two-flavored heavy) mesons have become one of the very active fields [50, 51, 52, 53, 54, 55, 56, 57, 58, 59, 60, 61, 62, 63, 64, 65, 66, 67]. Currently, experimental efforts to confirm the existence of  $B_c^*$  meson is probably one of the most important issues.

# Chapter 2

## Meson Mass-Shift Calculation

We interpret the mass shift as the in-medium Lorentz-scalar potential for the meson, and it is computed by the difference of the in-medium meson mass ( $m^*$ ) and the free space meson mass ( $m$ ):

$$V = m^* - m. \quad (2.1)$$

The mass shift of the mesons mentioned above are estimated by calculating the self-energies with the excitations of intermediate state mesons with light quarks  $u$  or  $d$ .

We employ an SU(5) effective Lagrangian (density) with minimal substitutions to get the interaction Lagrangians for calculating the self-energies of two-flavored heavy mesons in free space as well as in symmetric nuclear matter. The necessary inputs for calculating the in-medium meson self-energies are the effective masses (Lorentz-scalar) of the intermediate state mesons (the Lorentz-vector potentials cancel between the excited mesons appearing in the self-energy loop, and no need in the present study). The in-medium masses of the excited mesons appearing in the self-energy processes are calculated by the quark-meson coupling (QMC) model invented by Guichon [68].

### 2.1 The Quark-Meson Coupling Model

To get an insight in the internal structure change of hadrons in a nuclear medium, the QMC model plays a crucial role [69, 70, 71, 72, 73, 74, 75, 76, 77, 78, 79, 80, 81], similarly, for this project, the in-medium masses of mesons  $B, D$  and  $K$  ( $B^*, D^*$  and  $K^*$ ) were estimated using this model.

In this model, the relativistically moving, confined light quarks  $u$  and  $d$  (not the heavier  $s, c, b$  quarks) in the nucleon bag, interact self-consistently with the  $\sigma, \omega$  and  $\rho$  mean fields generated by the light quarks in the other nucleons including itself. The self-consistent response of the bound light quarks to the mean fields  $\sigma$  and  $\omega$  (also isovector field  $\rho$  in isospin asymmetric nuclear matter) leads to a new saturation mechanism for nuclear matter. Thus, in a nuclear medium, the internal structure of the nucleon is modified by the (light quark)-( $\sigma$  scalar meson) coupling, while the (light quark)-( $\omega$  vector meson) coupling shifts the energy. The Dirac equations for the light quarks ( $q = u, d$ ) and heavier quarks  $Q$  (see below after equations) are given by

$$\begin{aligned} & \left[ i\gamma \cdot \partial_x - (m_q - V_\sigma^q) \mp \gamma^0 \left( V_\omega^q + \frac{1}{2} V_\rho^q \right) \right] \begin{pmatrix} \psi_u(x) \\ \psi_{\bar{u}}(x) \end{pmatrix} = 0, \\ & \left[ i\gamma \cdot \partial_x - (m_q - V_\sigma^q) \mp \gamma^0 \left( V_\omega^q - \frac{1}{2} V_\rho^q \right) \right] \begin{pmatrix} \psi_d(x) \\ \psi_{\bar{d}}(x) \end{pmatrix} = 0, \\ & [i\gamma \cdot \partial_x - m_Q] \psi_{Q, \bar{Q}}(x) = 0, \end{aligned}$$

where  $Q = s, c$  or  $b$  hereafter (and the same way,  $\bar{q} = \bar{u}$ , or  $\bar{d}$  and  $\bar{Q} = \bar{s}, \bar{c}$  or  $\bar{b}$ ).

Note that only the light quarks  $u$  and  $d$ , feel the mean field potentials  $V_\sigma^q, V_\omega^q$  and  $V_\rho^q$ , where  $V_\sigma^q \equiv g_\sigma^q \sigma$ ,  $V_\omega^q \equiv g_\omega^q \omega$ ,  $V_\rho^q \equiv g_\rho^q b$ , with  $(g_\sigma^q, g_\omega^q, g_\rho^q)$  is the corresponding ( $q$ - $\sigma, q$ - $\omega, q$ - $\rho$ ) coupling constant. In other words, in the QMC model, the fields that directly couple to the light quarks are the Lorentz-scalar-isoscalar, Lorentz-vector-isoscalar and Lorentz-vector-isovector fields.

The eigenenergies for the quarks and antiquarks in a hadron  $h$  ( $= B, B^*, D, D^*, K$ , or  $K^*$ ) in units of the in-medium bag radius of hadron  $h$ ,  $1/R_h^*$ <sup>1</sup> are given by

$$\begin{pmatrix} \epsilon_u \\ \epsilon_{\bar{u}} \end{pmatrix} = \Omega_q^* \pm R_h^* \left( V_\omega^q + \frac{1}{2} V_\rho^q \right), \quad (2.2)$$

$$\begin{pmatrix} \epsilon_d \\ \epsilon_{\bar{d}} \end{pmatrix} = \Omega_q^* \pm R_h^* \left( V_\omega^q - \frac{1}{2} V_\rho^q \right), \quad (2.3)$$

$$\epsilon_{s,c,b} = \epsilon_{\bar{s},\bar{c},\bar{b}} = \Omega_{s,c,b}^*. \quad (2.4)$$

While the mass of a hadron  $h$  in symmetric nuclear matter  $m_h^*$  is calculated by,

$$m_h^* = \sum_{j=q,\bar{q},Q,\bar{Q}} \frac{n_j \Omega_j^* - Z_h}{R_h^*} + \frac{4}{3} \pi R_h^{*3} B_p, \quad \left. \frac{dm_h^*}{dR_h} \right|_{R_h=R_h^*} = 0. \quad (2.5)$$

---

<sup>1</sup>We indicate the in-medium quantity with an asterisk '\*\*', except for indicating the vector mesons,  $B^*, D^*, K^*, B_c^*, B_s^*$  and  $D_s^*$ , which may be clear.

where,  $\Omega_q^* = \Omega_{\bar{q}}^* = [x_q^2 + (R_h^* m_q^*)^2]^{1/2}$ ,  $m_q^* = m_q - g_\sigma^q \sigma$ ,  $\Omega_Q^* = \Omega_{\bar{Q}}^* = [x_Q^2 + (R_h^* m_Q)^2]^{1/2}$ , with  $x_{q,Q}^*$  being the lowest-mode bag eigenfrequencies,  $B_p$  is the bag constant (assumed to be independent of density),  $n_{q,Q}[n_{\bar{q}\bar{Q}}]$  are the lowest-mode valence quark numbers of each quark flavor in hadron  $h$ ,  $Z_h$  parametrizes the sum of the center of mass and gluon fluctuation effects (assumed to be independent of density). The current quark mass values used are  $(m_q, m_s, m_c, m_b) = (5, 250, 1270, 4200)$  MeV. (See Ref. [40] for the other values used,  $(m_q, m_s, m_c, m_b) = (5, 93, 1270, 4180)$  MeV.) The free space nucleon bag radius is chosen to be  $R_N = 0.8$  fm, and the light quark-meson coupling constants,  $g_\sigma^q$ ,  $g_\omega^q$  and  $g_\rho^q$ , are determined by the fit to the binding energy per nucleon of 15.7 MeV at the saturation density ( $\rho_0 = 0.15$  fm $^{-3}$ ) of symmetric nuclear matter, and the bulk symmetry energy (35 MeV) [68, 69, 70]. Bag constant  $B_p = (170 \text{ MeV})^4$  is determined by the free nucleon mass  $m_N = 939$  MeV which is the standard input values in the QMC model.

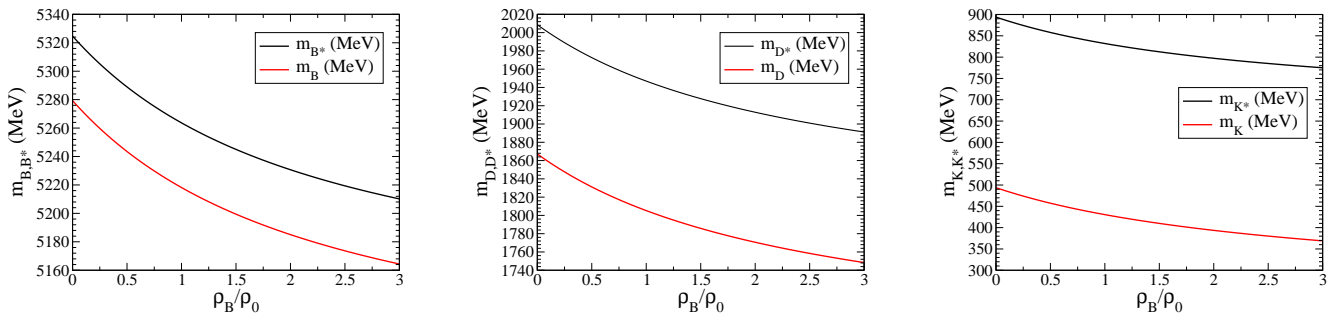


Figure 2.1:  $B$  and  $B^*$  (left panel),  $D$  and  $D^*$  (middle panel) and  $K$  and  $K^*$  (right panel) meson Lorentz-scalar effective masses in symmetric nuclear matter versus baryon density ( $\rho_B/\rho_0$ ), calculated by the QMC model.

In Fig. 2.1 it is presented the in-medium Lorentz-scalar effective masses of mesons  $B, B^*, D, D^*, K$  and  $K^*$ .

The QMC model predicts mass shift ( $\Delta m = m^* - m$ ) for these meson in symmetric nuclear matter at  $\rho_0$  ( $\Delta m_B, \Delta m_{B^*}, \Delta m_D, \Delta m_{D^*}, \Delta m_K, \Delta m_{K^*}$ ) =  $(-61.13, -61.05, -61.97, -61.66, -63.2, -61.97)$  MeV where  $\rho_0 = 0.15$  fm $^{-3}$ . We use these density dependence of the in-medium masses to estimate the self-energies of  $B_c, B_c^*, B_s, B_s^*, D_s$  and  $D_s^*$ .

## 2.2 Meson Self-Energy

Let us analyse the lowest one-loop order self-energy diagram of particle  $A$  depicted below.

1

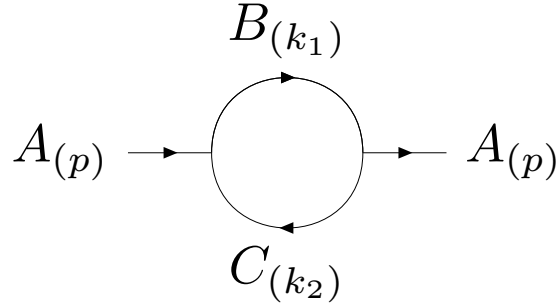


Figure 2.2: The lowest one-loop order self-energy of particle  $A$ . From the left- to right-direction we have an incoming particle  $A$  carrying a momentum ( $p$ ) which will reach the vertex and dissociate into two virtual particles denoted by  $B$  and  $C$  carrying a respective momentum  $k_1$  and  $k_2$  and finally recombine into  $A$  again.

Based on the self-energy process shown in Fig. 2.2, we are now in a position to explain specific cases relevant for our studies as follows: In Fig. 2.3 we show the self-energy loop graphs for mesons  $B_c$  (top),  $B_s$  (middle) and  $D_s$  (bottom). Our particular interest is at the left panel for each meson in Fig 2.3, because each of them presents a lighter total mass excitation in the corresponding meson self-energies, and thus we may naively expect that the left graph may be more dominant than the right graph in each horizontal panel. (However, the final results will show that this is not the case.)

We explicitly give the total mass values of the intermediate states corresponding to the graphs shown in Fig. 2.3:

$$(B^*, D) \rightarrow m_{B^*} + m_D = 7191.9 \text{ MeV}, \quad (B, D^*) \rightarrow m_B + m_{D^*} = 7287.9 \text{ MeV}, \quad (2.6)$$

$$(B^*, K) \rightarrow m_{B^*} + m_K = 5818.4 \text{ MeV}, \quad (B, K^*) \rightarrow m_B + m_{K^*} = 6173.3 \text{ MeV}, \quad (2.7)$$

$$(D^*, K) \rightarrow m_{D^*} + m_K = 2502.3 \text{ MeV}, \quad (D, K^*) \rightarrow m_D + m_{K^*} = 2761.1 \text{ MeV}. \quad (2.8)$$

By the above comparison, we note that from Eq. (2.6), the  $(B^*D)$  and  $(BD^*)$  cases, the total mass values are rather close, and some structure, Lorentz structure, pole position etc. may reverse our naive expectation. (In fact, it is the case as will be shown.)

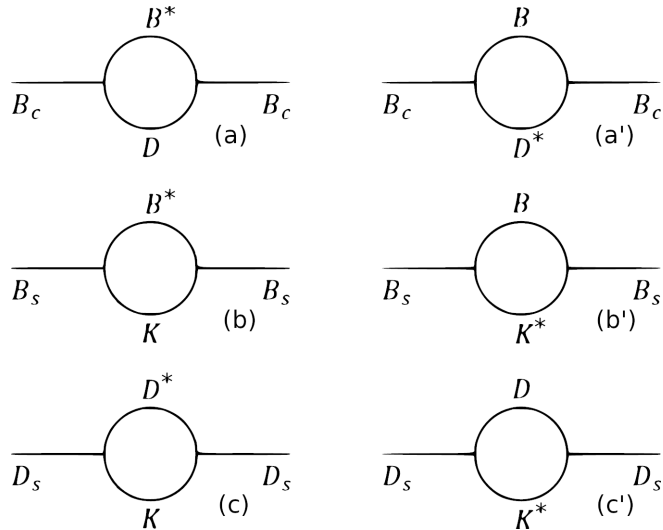


Figure 2.3: Pseudoscalar meson self-energies in two lighter meson excitations in the one-loop order, for  $B_c$  (top panel),  $B_s$  (middle panel), and  $D_s$  (bottom panel).

Similarly, we consider the self-energy graphs for the vector mesons  $B_c^*$ ,  $B_s^*$  and  $D_s^*$  depicted in Fig. 2.4

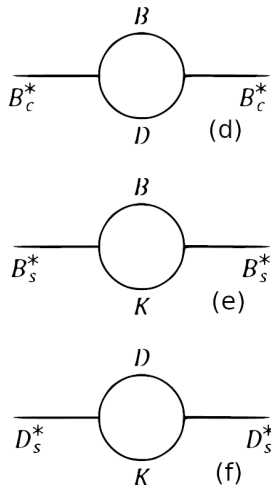


Figure 2.4: Vector meson self-energies for  $B_c^*$  (top panel),  $B_s^*$  (middle panel) and  $D_s^*$  (bottom panel) in the lowest order.

In the following we focus on the  $B_c$  and  $B_c^*$  mesons, respectively the top panel in Fig. 2.3, and the top panel in Fig 2.4. For the other meson self-energies in Figs. 2.3 and 2.4, we give the detailed results in later sections.

Note that, according to Ref. [52] the  $\Upsilon$  self-energy with the heavier  $B^*\bar{B}^*$  (VVV coupling, V: vector meson) gives unexpectedly large contribution, and we made our "min-

imal” predictions by avoiding this VVV coupling for the  $\Upsilon$  self-energy. We follow this practice, and we do not include possible  $B^*\bar{D}^*$  ( $\bar{B}^*D^*$ ) process in the self-energy for  $B_c^*$ . This will also enable us to compare with the present results with those of the  $\Upsilon$  and  $J/\Psi$  based on the same footing. Note that, clearly no VVV coupling for  $\eta_{b,c}$ , since they are pseudoscalar mesons, P.

## 2.3 Interaction Lagrangian

In the relevant self-energy loop graphs for the study, the vertex has a PPV interaction structure, which respects the parity conservation for the strong interaction.

To evaluate the self-energy loop graphs shown in Figs. 2.3 and 2.4, we start from a free SU(5) symmetric effective Lagrangian in the quark flavor space to obtain the interaction Lagrangian, and from there, we can compute the self-energies of the corresponding mesons.

The free Lagrangian of pseudoscalar (P) and vector (V) mesons based on the flavor SU(5) symmetry is given by [82, 83]:

$$\mathcal{L}_0 = Tr(\partial_\mu P^\dagger \partial^\mu P) - \frac{1}{2}Tr(F_{\mu\nu}^\dagger F^{\mu\nu})$$

where  $F_{\mu\nu} = \partial_\mu V_\nu - \partial_\nu V_\mu$ , and P and  $V_\mu$  are expressed by  $5 \times 5$  matrices which are obtained by using the generators of SU(5) (see Appendix B) as  $P_j^i = 1/\sqrt{2}(\lambda_a)_j^i \phi_a$  and  $V_{\mu j}^i = 1/\sqrt{2}(\lambda_a)_j^i v_{\mu a}$ . Here  $\phi_a$  is the Cartesian component of pseudoscalar meson fields ( $a = 1, \dots, 24$ ) entering in the expression  $P_j^i$ , and  $v_{\mu a}$  is again the Cartesian component of the vector meson fields entering  $V_{\mu j}^i$ , and  $\lambda_a$  are the SU(5) version of "Gell-Mann matrices" ( $a = 1, \dots, 24$ ), and  $i$  and  $j$  are matrix indices (see Appendix B).

Then P and V (suppressing Lorentz indices) are expressed by the physical meson fields:

$$P = \frac{1}{\sqrt{2}} \begin{pmatrix} \frac{\pi^0}{\sqrt{2}} + \frac{\eta}{\sqrt{6}} + \frac{\eta_c}{\sqrt{12}} + \frac{\eta_b}{\sqrt{20}} & \pi^+ & K^+ & \bar{D}^0 & B^+ \\ \pi^- & \frac{-\pi^0}{\sqrt{2}} + \frac{\eta}{\sqrt{6}} + \frac{\eta_c}{\sqrt{12}} + \frac{\eta_b}{\sqrt{20}} & K^0 & D^- & B^0 \\ K^- & \bar{K}^0 & \frac{-2\eta}{\sqrt{6}} + \frac{\eta_c}{\sqrt{12}} + \frac{\eta_b}{\sqrt{20}} & D_s^- & B_s^0 \\ D^0 & D^+ & D_s^+ & \frac{-3\eta_c}{\sqrt{12}} + \frac{\eta_b}{\sqrt{20}} & B_c^+ \\ B^- & \bar{B}^0 & \bar{B}_s^0 & B_c^- & \frac{-2\eta_b}{\sqrt{5}} \end{pmatrix}, \quad (2.9)$$

$$V = \frac{1}{\sqrt{2}} \begin{pmatrix} \frac{\rho^0}{\sqrt{2}} + \frac{\omega}{\sqrt{6}} + \frac{J/\Psi}{\sqrt{12}} + \frac{\Upsilon}{\sqrt{20}} & \rho^+ & K^{*+} & \bar{D}^{*0} & B^{*+} \\ \rho^- & \frac{-\rho^0}{\sqrt{2}} + \frac{\omega}{\sqrt{6}} + \frac{J/\Psi}{\sqrt{12}} + \frac{\Upsilon}{\sqrt{20}} & K^{*0} & D^{*-} & B^{*0} \\ K^{*-} & \bar{K}^{*0} & \frac{-2\omega}{\sqrt{6}} + \frac{J/\Psi}{\sqrt{12}} + \frac{\Upsilon}{\sqrt{20}} & D_s^{*-} & B_s^{*0} \\ D^{*0} & D^{*+} & D_s^{*+} & \frac{-3J/\Psi}{\sqrt{12}} + \frac{\Upsilon}{\sqrt{20}} & B_c^{*+} \\ B^{*-} & \bar{B}^{*0} & \bar{B}_s^{*0} & B_c^{*-} & \frac{-2\Upsilon}{\sqrt{5}} \end{pmatrix}. \quad (2.10)$$

where we use the following conventions,

$$K = \begin{pmatrix} K^+ \\ K^0 \end{pmatrix} = \begin{pmatrix} u\bar{s} \\ d\bar{s} \end{pmatrix}, \quad \bar{K} \equiv K^\dagger = \begin{pmatrix} K^- & \bar{K}^0 \end{pmatrix} = \begin{pmatrix} \bar{u}s & \bar{d}s \end{pmatrix},$$

$$\bar{D} = \begin{pmatrix} \bar{D}^0 \\ D^- \end{pmatrix} = \begin{pmatrix} u\bar{c} \\ d\bar{c} \end{pmatrix}, \quad D \equiv (\bar{D})^\dagger = \begin{pmatrix} D^0 & D^+ \end{pmatrix} = \begin{pmatrix} \bar{u}c & \bar{d}c \end{pmatrix},$$

$$B = \begin{pmatrix} B^+ \\ B^0 \end{pmatrix} = \begin{pmatrix} u\bar{b} \\ d\bar{b} \end{pmatrix}, \quad \bar{B} \equiv B^\dagger = \begin{pmatrix} B^- & \bar{B}^0 \end{pmatrix} = \begin{pmatrix} \bar{u}b & \bar{d}b \end{pmatrix}.$$

Note that, in addition, similar conventions are used for the vector mesons  $K^*$ ,  $D^*$ , and  $B^*$ , each corresponding to  $K$ ,  $D$  and  $B$  above.

Transformation of these tensors  $P_j^i$  and  $V_j^i$  under SU(5) transformation are given by,

$$P_j^i \rightarrow U_{ia} P_b^a U_j^{\dagger b}, \quad (2.11)$$

and

$$V_j^i \rightarrow U_{ia} V_b^a U_j^{\dagger b}, \quad (2.12)$$

where,  $P_b^a$  and  $V_{\mu b}^a$  are the matrix representations of the pseudo-scalar and the vector mesons (irreducible tensors), and they are obtained using the SU(5) generators with adjoint representation (matrix representation/notation) by rewriting from the Cartesian components to physical components. (See Appendix B.)

## 2.4 Self-energy Calculation

By the minimal substitutions [82]:

$$\partial_\mu P \rightarrow D_\mu P = \partial_\mu P - \frac{ig}{2} [V_\mu, P], \quad (2.13)$$

$$F_{\mu\nu} \rightarrow F_{\mu\nu} - \frac{ig}{2}[V_\mu, V_\nu], \quad (2.14)$$

we get the interaction Lagrangian:

$$\mathcal{L} = \mathcal{L}_0 + ig \text{Tr}(\partial^\mu P [P, V_\nu]) - \frac{g^2}{4} \text{Tr}([P, V_\mu]^2) + ig \text{Tr}(\partial^\mu V^\nu [V_\mu, V_\nu]) + \frac{g^2}{8} \text{Tr}([V_\mu, V_\nu]^2). \quad (2.15)$$

In Eq. (2.15)  $\mathcal{L}_0$  represents the free Lagrangian, while the interaction terms describe the pseudoscalar(P)-pseudoscalar(P)-vector(V) (PPV), PPVV, VVV and VVVV couplings. For the self-energy diagrams shown in Figs. 2.3 and 2.4, only the second term in Eq. (2.15), PPV coupling, is necessary.

For example, the second term of  $\mathcal{L}_{B_c^*BD}$  can be obtained performing  $\text{Tr} \partial_\mu P (PV^\mu - V^\mu P)$  but, to do that, we use the P and V matrices, keeping only the terms that are involved in the interaction:

$$P = \frac{1}{\sqrt{2}} \begin{pmatrix} 0 & 0 & 0 & \overline{D}^0 & B^+ \\ 0 & 0 & 0 & D^- & B^0 \\ 0 & 0 & 0 & 0 & 0 \\ D^0 & D^+ & 0 & 0 & 0 \\ B^- & \overline{B}^0 & 0 & 0 & 0 \end{pmatrix},$$

$$V = \frac{1}{\sqrt{2}} \begin{pmatrix} 0 & 0 & 0 & 0 & 0 \\ 0 & 0 & 0 & 0 & 0 \\ 0 & 0 & 0 & 0 & 0 \\ 0 & 0 & 0 & 0 & B_c^{*+} \\ 0 & 0 & 0 & B_c^{*-} & 0 \end{pmatrix}.$$

Then,  $\text{Tr} \partial_\mu P (PV^\mu - V^\mu P)$  gives:

$$\begin{aligned} \text{Tr} \partial_\mu P (PV^\mu - V^\mu P) = & [-(\partial_\mu \overline{D}^0 B_c^{*+} B^-) - (\partial_\mu B^+ B_c^{*-} D^0)] \\ & + [-(\partial_\mu D^- B_c^{*+} \overline{B}^0) - (\partial_\mu B^0 B_c^{*-} D^+)] \\ & + [(\partial_\mu D^0 B^+ B_c^{*-}) + (\partial_\mu D^+ B^0 B_c^-)] \\ & + [(\partial_\mu B^- \overline{D}^0 B_c^{*+}) + (\partial_\mu \overline{B}^0 D^- B_c^{*+})]. \end{aligned} \quad (2.16)$$

Performing the trace in the above, we get the interaction Lagrangian for  $B_c$ :

$$\mathcal{L}_{B_c^*BD} = -ig_{B_c^*BD} [B(\partial_\mu \overline{D}) - (\partial_\mu B) \overline{D}] B_c^{*\mu} + h.c.$$

Finally, for the set of interaction terms required to study the interactions of  $B_c$ ,  $B_s$ , and  $D_s$  and  $B_c^*$ ,  $B_s^*$  and  $D_s^*$  we get:

$$\mathcal{L}_{B_c B^* D} = ig_{B_c B^* D} [(\partial_\mu B_c^-)D - B_c^- (\partial_\mu D)] B^{*\mu} + h.c. \quad (2.17)$$

$$\mathcal{L}_{B_c B D^*} = ig_{B_c B D^*} [(\partial_\mu B_c^+) \bar{B} - B_c^+ (\partial_\mu \bar{B})] \bar{D}^{*\mu} + h.c. \quad (2.18)$$

$$\mathcal{L}_{B_s B^* K} = ig_{B_s B^* K} [(\partial_\mu \bar{B}_s^0) \bar{K} - \bar{B}_s^0 (\partial_\mu \bar{K})] B^{*\mu} + h.c. \quad (2.19)$$

$$\mathcal{L}_{B_s B K^*} = ig_{B_s B K^*} [(\partial_\mu B_s^0) \bar{B} - B_s^0 (\partial_\mu \bar{B})] K^{*\mu} + h.c. \quad (2.20)$$

$$\mathcal{L}_{D_s D^* K} = ig_{D_s D^* K} [(\partial_\mu D_s^+) \bar{K} - D_s^+ (\partial_\mu \bar{K})] \bar{D}^{*\mu} + h.c. \quad (2.21)$$

$$\mathcal{L}_{D_s D K^*} = ig_{D_s D K^*} [(\partial_\mu D_s^-) D - D_s^- (\partial_\mu D)] K^{*\mu} + h.c. \quad (2.22)$$

$$\mathcal{L}_{B_c^* B D} = -ig_{B_c^* B D} B_c^{*+\mu} [\bar{B} (\partial_\mu \bar{D}) - (\partial_\mu \bar{B}) \bar{D}] + h.c. \quad (2.23)$$

$$\mathcal{L}_{B_s^* B K} = -ig_{B_s^* B K} B_s^{*0\mu} [\bar{B} (\partial_\mu K) - (\partial_\mu \bar{B}) K] + h.c. \quad (2.24)$$

$$\mathcal{L}_{D_s^* D K} = -ig_{D_s^* D K} D_s^{*-\mu} [D (\partial_\mu K) - (\partial_\mu D) K] + h.c. \quad (2.25)$$

With these interaction Lagrangians, we can calculate self-energy graphs, that results in the Lorentz scalar effective meson mass, or potential  $V_s$ , for the corresponding mesons. Note that, for the quarks  $s, c$  and  $b$ , the present approach assumes that there arises no "Lorentz vector", in-medium potentials based on the QMC model. (See Ref. [68, 80, 81].)

Based on the vector meson dominance (VMD) hypothesis and experimental data of  $\Gamma(\Upsilon \rightarrow e^+ e^-)$  we have calculated the coupling constant  $g_{\Upsilon BB}$  [82] (see Appendix C).

$$g_{\Upsilon BB} = g_{\Upsilon B^* B} = \frac{5g}{4\sqrt{10}} \approx 13.2 \quad (2.26)$$

Using Eq. (2.26) [48, 52] we obtain  $g \approx 33.45$ , and the relevant coupling constants by:

$$g_{B_c B D^*} = g_{B_c B^* D} = g_{B_c^* B D} = \frac{g}{2\sqrt{2}}, \quad (2.27)$$

$$g_{B_c B D^*} = g_{B_c B^* D} = g_{B_c B_s D_s^*} = g_{B_c B_s^* D_s} = \frac{g}{2\sqrt{2}}, \quad (2.28)$$

$$g_{K D^* D_s} = g_{K D D_s^*} = g_{K B^* D_s} = g_{K B B_s^*} = \frac{g}{2\sqrt{2}}. \quad (2.29)$$

Thus, we get  $g_{B_c B D^*} = g_{B_c B^* D} \approx 11.9$

We must, however, draw attention to the coupling constant used in the present work. To obtain the above value, we use the experimental data from the  $\Upsilon$  decay, although we could instead perform a similar calculation using the experimental data from the  $J/\Psi$

decay, which would lead us to obtain a different value for  $g_{B_c B D^*}(g_{B_c B^* D})$ . It, of course, would imply in different numerical values for all results, but all the relative relations would remain the same.

In the following we simplify the effective Lagrangians for  $B_c$  and  $B_c^*$ . In order to pay attention and emphasize some points, there are terms with underlines in the Lagrangians throughout hereafter.

$$\mathcal{L}_{B_c B^* D} = ig_{B_c B^* D} \overline{B}_\mu^* [\underline{B_c^+}(\partial^\mu \overline{D}) - (\partial^\mu B_c^+) \overline{D}] - ig_{B_c B^* D} [\underline{B_c^-}(\partial^\mu D) - (\partial^\mu B_c^-) D] B_\mu^* \quad (2.30)$$

$$\mathcal{L}_{D B B_c^*} = ig_{D B B_c^*} B_{c\mu}^{*+} [(\partial^\mu \overline{B}) \overline{D} - \underline{\overline{B}(\partial^\mu \overline{D})}] - ig_{D B B_c^*} B_{c\mu}^{*-} [\overline{D}(\partial^\mu \overline{B}) - \underline{(\partial^\mu \overline{D}) \overline{B}}] \quad (2.31)$$

Integrating by parts the underlined terms and dropping the surface terms ( $= 0$ ), and using Lorenz condition  $\partial^\mu B_\mu^*$  and  $\partial^\mu \overline{B}_\mu^* = 0$ , we get the simplified expressions for the  $B_c$  interaction Lagrangian,

$$\mathcal{L}_{B_c B^* D} = 2ig_{B_c B^* D} [-(\partial^\mu B_c^+) \overline{B}_\mu^* \overline{D} + (\partial^\mu B_c^-) D B_\mu^*], \quad (2.32)$$

and for  $B_c^*$ ,

$$\mathcal{L}_{D B B_c^*} = 2ig_{D B B_c^*} [B_{c\mu}^{*+} (\partial^\mu \overline{B}) \overline{D} - B_{c\mu}^{*-} D (\partial^\mu B)]. \quad (2.33)$$

The explicit use of meson doublet fields are:

$$\overline{B}_\mu^* \overline{D} = \begin{pmatrix} B_\mu^{*-} & \overline{B}_\mu^{*0} \end{pmatrix} \begin{pmatrix} \overline{D}^0 \\ D^- \end{pmatrix} = B_\mu^{*-} \overline{D}^0 + \overline{B}_\mu^{*0} D^-,$$

$$D B = \begin{pmatrix} D^0 & D^+ \end{pmatrix} \begin{pmatrix} B^+ \\ B^0 \end{pmatrix} = D^0 B^+ + D^+ B^0,$$

and

$$\overline{B D} = \begin{pmatrix} B^- & \overline{B}^0 \end{pmatrix} \begin{pmatrix} \overline{D}^0 \\ D^- \end{pmatrix} = B^- \overline{D}^0 + \overline{B}^0 D^-,$$

$$D B = \begin{pmatrix} D^0 & D^+ \end{pmatrix} \begin{pmatrix} B^+ \\ B^0 \end{pmatrix} = D^0 B^+ + D^+ B^0.$$

From the general expression for scattering matrix,  $S$ :

$$\begin{aligned} S &= 1 - i\mathcal{T}, \\ &= 1 - (2\pi)^4 \delta^{(4)}(p_f - p_i) i\mathcal{M}, \\ &= 1 + (2\pi)^4 \delta^{(4)}(p_f - p_i) (-i\mathcal{M}), \end{aligned} \quad (2.34)$$

where  $\mathcal{T}$  and  $\mathcal{M}$  are respectively the transition matrix and invariant amplitude, and we can define,  $-i\mathcal{M} = -i\Sigma$  and, therefore  $\mathcal{M} = \Sigma$  with  $\Sigma$  to be associated with the self-energy.

We calculate the lowest order non-trivial  $S$  matrix (second order for the connected processes) for  $B_c$  and  $B_c^*$  below.

For  $B_c$ ,

$$S_2 = \langle B_c^+(p) | T \frac{i^2}{2!} \int d^4x d^4y \mathcal{L}_{B_c B^* D}^{(x)} \mathcal{L}_{B_c B^* D}^{(y)} | B_c^+(p) \rangle, \quad (2.35)$$

and for  $B_c^*$ ,

$$S_2 = \langle B_{c\mu}^{*+}(p) | T \frac{i^2}{2!} \int d^4x d^4y \mathcal{L}_{DBB_c^*}^{(x)} \mathcal{L}_{DBB_c^*}^{(y)} | B_{c\nu}^{*+}(p) \rangle. \quad (2.36)$$

By exchanging the integral variables  $x \leftrightarrow y$ , and summing the terms which give the same contributions, we get the following expressions.

For  $B_c$ ,

$$S_2 = -4g_{B_c B^* D}^2 \int d^4x d^4y \langle 0 | (e^{ip \cdot x}) T [\underline{\overline{B}_\mu D}]_{(x)} [\underline{DB_\nu^*}]_{(y)} (e^{-ip \cdot x}) | 0 \rangle p^\mu p^\nu, \quad (2.37)$$

and for  $B_c^*$ ,

$$S_2 = \langle 0 | T \int d^4x d^4y (\epsilon_\mu^*(\lambda) e^{ip \cdot x}) \cdot 4g_{DBB_c^*}^2 [\underline{-D(\partial_x^\mu B)}]_{(x)} [\underline{(\partial_y^\nu \overline{B}) \overline{D}}]_{(y)} (\epsilon_\nu^*(\lambda) e^{-ip \cdot x}) | 0 \rangle. \quad (2.38)$$

Expanding the underlined terms in Eqs. (2.37) and (2.38), Feynman propagators show up as Eqs. (2.39), (2.40), (2.41), and (2.42) below.

For  $B_c$ ,

$$i\Delta_D(x-y) = i \int \frac{d^4\kappa_1}{(2\pi)^4} \frac{e^{-i\kappa_1 \cdot (x-y)}}{\kappa_1^2 - m_D^2 + i\epsilon}, \quad (2.39)$$

and

$$i\Delta_{B_{\mu\nu}^*}(x-y) = i \int \frac{d^4\kappa_2}{(2\pi)^4} \frac{(-g_{\mu\nu} + \kappa_{2\mu}\kappa_{2\nu}/m_{B^*}^2) e^{-i\kappa_2 \cdot (x-y)}}{\kappa_2^2 - m_{B^*}^2 + i\epsilon}. \quad (2.40)$$

In addition, for  $B_c^*$ , also appear,

$$i\Delta_B(x-y) = i \int \frac{d^4\kappa_2}{(2\pi)^4} \frac{e^{-i\kappa_2 \cdot (x-y)}}{\kappa_2^2 - m_B^2 + i\epsilon}, \quad (2.41)$$

and

$$i\Delta_D(x-y) = i \int \frac{d^4\kappa_1}{(2\pi)^4} \frac{e^{-i\kappa_1 \cdot (x-y)}}{\kappa_1^2 - m_D^2 + i\epsilon}. \quad (2.42)$$

Inserting the above expressions into expressions for  $S_2$ , Eqs. (2.37), and (2.38), we obtain:

For  $B_c$ ,

$$S_2 = \int d^4x d^4y (-4g_{B_c B^* D}^2) e^{-ip \cdot y} e^{ip \cdot x} \cdot 2(p^\mu p^\nu) \\ \times i \int \frac{d^4\kappa_1}{(2\pi)^4} \frac{e^{-i\kappa_1 \cdot (x-y)}}{\kappa_1^2 - m_D^2 + i\epsilon} i \int \frac{d^4\kappa_2}{(2\pi)^4} \frac{(-g_{\mu\nu} + \kappa_{2\mu}\kappa_{2\nu})/m_{B^*}^2}{\kappa_2^2 - m_{B^*}^2 + i\epsilon} e^{-i\kappa_2 \cdot (x-y)}, \quad (2.43)$$

and for  $B_c^*$ ,

$$S_2 = \int d^4x d^4y \epsilon_\mu^*(\lambda) \epsilon_\nu(\lambda) e^{ip \cdot x} e^{-ip \cdot y} (4g_{DBB_c^*}^2) \\ \times 2 \int \frac{d^4\kappa_1}{(2\pi)^4} \frac{e^{-i\kappa_1 \cdot (x-y)}}{\kappa_1^2 - m_D^2 + i\epsilon} \int \frac{d^4\kappa_2}{(2\pi)^4} \frac{\partial_\mu^x \partial_\nu^y e^{-i\kappa_2 \cdot (x-y)}}{\kappa_2^2 - m_B^2 + i\epsilon}. \quad (2.44)$$

With  $p = \kappa_1 + \kappa_2$ ,  $\kappa_2 \equiv \kappa \rightarrow \kappa_1 = p - \kappa$ , we obtain:

For  $B_c$ ,

$$S_2 = 8g_{B_c B^* D}^2 (p^\mu p^\nu) \int \frac{d^4\kappa}{(2\pi)^4} \frac{(-g_{\mu\nu} + \kappa_\mu \kappa_\nu / m_{B^*}^2)}{\kappa^2 - m_{B^*}^2 + i\epsilon} \frac{1}{(p - \kappa)^2 - m_D^2 + i\epsilon} (2\pi)^4 \delta^{(4)}(p - p), \quad (2.45)$$

and for  $B_c^*$ ,

$$S_2 = 8g_{B_c^* B D}^2 \int \frac{d^4\kappa}{(2\pi)^4} \kappa^\mu \kappa^\nu \epsilon_\mu^*(\lambda) \epsilon_\nu(\lambda) \frac{1}{\kappa^2 - m_B^2 + i\epsilon} \frac{1}{(p - \kappa)^2 - m_D^2 + i\epsilon} (2\pi)^4 \delta^{(4)}(p - p) \quad (2.46)$$

Since,  $-i\mathcal{M} = -i\Sigma$ , then we obtain:

For  $B_c$ ,

$$\Sigma_{B_c}^{B^* D}(p) = -\frac{1}{i} 8g_{B_c B^* D}^2 (p^\mu p^\nu) \int \frac{d^4\kappa}{(2\pi)^4} \frac{(-g_{\mu\nu} + \kappa_\mu \kappa_\nu / m_{B^*}^2)}{\kappa^2 - m_{B^*}^2 + i\epsilon} \frac{1}{(p - \kappa)^2 - m_D^2 + i\epsilon} (2\pi)^4 \delta^{(4)}(p - p), \quad (2.47)$$

and for  $B_c^*$ ,

$$\Sigma_{B_c^*}^{BD}(p) = -\frac{1}{i} 8g_{DBB_c^*}^2 \int \frac{d^4\kappa}{(2\pi)^4} \kappa^\mu \kappa^\nu \epsilon_\mu^*(\lambda) \epsilon_\nu(\lambda) \frac{1}{\kappa^2 - m_B^2 + i\epsilon} \frac{1}{(p - \kappa)^2 - m_D^2 + i\epsilon} (2\pi)^4 \delta^{(4)}(p - p). \quad (2.48)$$

Note that, although we estimate the mass shift of  $B_c^*$  meson, the existence is suggested by theoretically and the existence has not yet been confirmed by experiment. We emphasize that, our study brings the first predictions for the mass shift of both the  $B_c$  and  $B_c^*$  mesons in a nuclear medium (many nucleon system).

Similar calculations can also be done for  $B_s$ ,  $D_s$  pseudo-scalar mesons, as well as for  $B_s^*$ , and  $D_s^*$  vector mesons. Of course, all the estimates for the mass shift of these mesons are our predictions, and are made for the first time, which means, no one has ever calculated/estimated.

We first calculate the free space physical meson mass,

$$m^2 = (m^0)^2 - |\Sigma(p^2 = m^2)|, \quad (2.49)$$

where  $m^0$  is the bare mass,  $p$  is the meson four-momentum,  $\Sigma$  the total self-energy in free space which is the sum of each loop contribution in free space. (See Figs. 2.3 and 2.4.) To make clear the sign convention, we introduced the modulus as  $|\Sigma|$ , based on the fact that "the second-order perturbation gives always the negative contribution for the energy (mass) with the virtual state excitations". According to Eq. (2.49), we fix the  $m^0$  value by the free space physical meson mass  $m$ . To calculate the in-medium meson mass  $m^*$ , we use this fixed  $m^0$  value, together with the in-medium self-energy  $\Sigma^*$  corresponding to Eq. (2.49).

In symmetric nuclear matter rest frame, we consider the  $B_c$  meson at rest,  $p^\mu = (m_{B_c}^*, \vec{0})$ . The numerator  $(-g_{\mu\nu} + \kappa_\mu \kappa_\nu)/m_{B^*}^{*2}$  of  $B^*$  meson propagator in Eq. (2.47) can then be evaluated in this rest frame:

$$\begin{aligned} p^\mu p^\nu (-g_{\mu\nu} + \kappa_\mu \kappa_\nu)/m_{B^*}^{*2} &= -p^2 + (p \cdot \kappa)(p \cdot \kappa)/m_{B^*}^{*2}, \\ &= -m_{B_c}^{*2} + (m_{B_c}^* \kappa_0^*)(m_{B_c}^* \kappa_0^*)/m_{B^*}^{*2}, \\ &= m_{B_c}^{*2} (-1 + \kappa_0^{*2}/m_{B^*}^{*2}), \\ &= \left(\frac{m_{B_c}^{*2}}{m_{B^*}^{*2}}\right) (-m_{B^*}^{*2} + k_0^{*2}), \\ &= \left(\frac{m_{B_c}^{*2}}{m_{B^*}^{*2}}\right) ((\kappa_0 + V)^2 - m_{B^*}^{*2}), \\ &= \left(\frac{m_{B_c}^{*2}}{m_{B^*}^{*2}}\right) (\kappa_0 + V + m_{B^*}^*)(\kappa_0 + V - m_{B^*}^*). \end{aligned} \quad (2.50)$$

In the above,  $V$  stands for the time component of the vector-mean field potential which comes from the QMC model approach, and adds to the time component of the in-medium energy as  $\kappa_0^* = \kappa_0 + V$ . See Refs. [69, 70, 71] and Appendix B for details. As for  $B_c^*$  meson,  $B_c^*$  since is a vector meson, its spin average is  $1/(2J+1) = 1/3$ , and in the

rest frame of  $B_c^*$  (in free space), since  $p^\mu = (m_{B_c^*}, \vec{0})$ , we get,

$$\begin{aligned}
\frac{1}{3} \sum_{spins} \kappa^\mu \kappa^\nu \epsilon_\mu^*(\lambda) \epsilon_\nu(\lambda) &= \frac{1}{3} (-g_{\mu\nu} + \frac{p_\mu p_\nu}{m_{B_c^*}^2}) \kappa^\mu \kappa^\nu, \\
&= \frac{1}{3} (-\kappa^2 + \frac{1}{m_{B_c^*}^2} (p_0 k^0) (p_0 k^0)), \\
&= \frac{1}{3} (-\kappa^2 + \frac{1}{m_{B_c^*}^2} m_{B_c^*}^2 (k^0)^2), \\
&= \frac{1}{3} (-(\kappa^0)^2 + \vec{\kappa}^2 + (\kappa^0)^2), \\
&= \frac{1}{3} |\vec{\kappa}^2|.
\end{aligned} \tag{2.51}$$

where in the first term, it corresponds to  $\frac{1}{2J+1} \sum_{spins}$ . Furthermore,

$$\begin{aligned}
\int \frac{d^4 \kappa}{(2\pi)^3} &= \int \frac{d^3 \kappa}{(2\pi)^3} \int \frac{d\kappa^0}{2\pi}, \\
&= \int \frac{d|\vec{\kappa}| 4\pi |\vec{\kappa}|^2}{(2\pi)^3} \int \frac{d\kappa^0}{2\pi}, \\
&= \frac{1}{2\pi^2} \int d|\vec{\kappa}| |\vec{\kappa}|^2 \int \frac{d\kappa^0}{2\pi}.
\end{aligned} \tag{2.52}$$

Thus, we get the expressions for  $B_c$  and for  $B_c^*$ :

$$\begin{aligned}
\Sigma_{B_c}^{B^*B}(m_{B_c}) &= \frac{-4g_{B_c B^* D}^2}{\pi^2} \int d|\vec{\kappa}| |\vec{\kappa}|^2 \\
&\times \int \frac{d\kappa_0}{2\pi i} \left( \frac{m_{B_c}^{*2}}{m_{B^*}^2} \right) \frac{(\kappa_0 + V + m_{B^*})(\kappa_0 + V - m_{B^*})}{\kappa^2 - m_{B^*}^2 + i\epsilon} \frac{1}{(p - \kappa)^2 - m_D^2 + i\epsilon},
\end{aligned} \tag{2.53}$$

$$\Sigma_{B_c^*}^{BD}(m_{B_c^*}) = \frac{-4g_{D B B_c^*}^2}{3\pi^2} \int d|\vec{\kappa}| |\vec{\kappa}|^4 \int \frac{d\kappa^0}{2\pi i} \frac{1}{\kappa^2 - m_B^2 + i\epsilon} \frac{1}{(p - \kappa)^2 - m_D^2 + i\epsilon}. \tag{2.54}$$

Therefore the in-medium self-energies are given by (the relevant meson masses are replaced by those of in medium):

For  $B_c$ ,

$$\begin{aligned}
\Sigma_{B_c}^{B^*B}(m_{B_c}^*) &= \frac{-4g_{B_c B^* D}^2}{\pi^2} \int d|\vec{\kappa}| |\vec{\kappa}|^2 \\
&\times \int \frac{d\kappa_0}{2\pi i} \left( \frac{m_{B_c}^{*2}}{m_{B^*}^{*2}} \right) \frac{(\kappa_0 + V + m_{B^*}^*)(\kappa_0 + V - m_{B^*}^*)}{\kappa^2 - m_{B^*}^{*2} + i\epsilon} \frac{1}{(p - \kappa)^2 - m_D^{*2} + i\epsilon},
\end{aligned} \tag{2.55}$$

and for  $B_c^*$ ,

$$\Sigma_{B_c^*}^{BD}(m_{B_c^*}^*) = \frac{-4g_{B_c^* B D}^2}{3\pi^2} \int d|\vec{\kappa}| |\vec{\kappa}|^4 \int \frac{d\kappa^0}{2\pi i} \frac{1}{\kappa^2 - m_B^{*2} + i\epsilon} \frac{1}{(p - \kappa)^2 - m_D^{*2} + i\epsilon}. \tag{2.56}$$

In order to evaluate the poles in the integral, we define:

For  $B_c$ ,

$$I_{B_c}^{B^*D} = \left(\frac{m_{B_c}^{*2}}{m_{B^*}^{*2}}\right) \int \frac{d\kappa_0}{2\pi i} \frac{(\kappa_0 + V + m_{B^*}^*)(\kappa_0 + V - m_{B^*}^*)}{\kappa^2 - m_{B^*}^{*2} + i\epsilon} \frac{1}{(p - \kappa)^2 - m_D^{*2} + i\epsilon}, \quad (2.57)$$

and for  $B_c^*$ ,

$$I_{B_c^*}^{BD} = \int \frac{1}{\kappa^2 - m_{B^*}^{*2} + i\epsilon} \frac{1}{(p - k)^2 - m_D^{*2} + i\epsilon}. \quad (2.58)$$

Inserting  $\kappa_0 = -\omega_B^*$  and  $\kappa_0 = m_{B_c}^* - \omega_D^*$ , and performing the Cauchy integral in the complex plane for  $\kappa_0$ ,  $I_{B_c}^{B^*D}$  and  $I_{B_c^*}^{BD}$  become:

For  $B_c$ ,

$$I_{B_c}^{B^*D}(|\vec{k}|) \equiv \left(\frac{m_{B_c}^2}{m_{B^*}^2}\right) \cdot \left[ \frac{(-\omega_{B^*}^* + m_{B^*}^*)(-\omega_{B^*}^* - m_{B^*}^*)}{(-2\omega_{B^*}^*)(-\omega_{B^*}^* - m_{B_c}^* + \omega_D^*)(-\omega_{B^*}^* - m_{B_c}^* - \omega_D^*)} + \frac{(m_{B_c}^* - \omega_D^* + m_{B^*}^*)(m_{B_c}^* - \omega_D^* - m_{B^*}^*)}{(m_{B_c}^* - \omega_D^* + \omega_{B^*}^*)(m_{B_c}^* - \omega_D^* - \omega_{B^*}^*)(-2\omega_D^*)} \right], \quad (2.59)$$

and for  $B_c^*$ ,

$$I_{B_c^*}^{BD}(|\vec{k}|) = \frac{1}{(-2\omega_B^*)(-\omega_B^* - m_{B_c^*}^* + \omega_D^*)(-\omega_B^* - m_{B_c^*}^* - \omega_D^*)} + \frac{1}{(m_{B_c^*}^* - \omega_D^* + \omega_B^*)(m_{B_c^*}^* - \omega_D^* - \omega_B^*)(-2\omega_D^*)}. \quad (2.60)$$

Finally. the self-energies of  $B_c$  and  $B_c^*$  can be expressed as:

For  $B_c$ ,

$$\Sigma_{B_c}^{B^*D}(m_{B_c}^{*2}) = \frac{-4g_{B_c B^* D}^2}{\pi^2} \int d|\vec{k}| |\vec{k}|^2 I_{B_c}^{B^*D}(|\vec{k}|), \quad (2.61)$$

and for  $B_c^*$ ,

$$\Sigma_{B_c^*}^{BD}(m_{B_c^*}^{*2}) = \frac{-4g_{B_c^* B D}^2}{3\pi^2} \int d|\vec{k}| |\vec{k}|^4 I_{B_c^*}^{BD}(|\vec{k}|). \quad (2.62)$$

It is straightforward to repeat the processes shown above to find the self-energies of pseudoscalar mesons,  $B_c$ ,  $B_s$ , and  $D_s$ , as well as of vector mesons  $B_c^*$ ,  $B_s^*$ , and  $D_s^*$ .

Note that the total the self-energy  $\Sigma_{B_c}$  is calculated summing both loop contributions in free space and ignoring the possible width (imaginary part) in self-energy.

Similar to Eq. (2.49) the in-medium mass is calculated using the same bare mass value  $m_{B_c}^0$  determined in free space with the in medium masses, for example,

$$m_{B_c}^2 = [m_{B_c}^0(B^*D + BD^*)]^2 - |\Sigma_{B_c}(B^*D) + \Sigma_{B_c}(BD^*)|(\kappa^2 = m_{B_c}^2), \quad (2.63)$$

$$m_{B_c}^{*2} = [m_{B_c}^0(B^*D + BD^*)]^2 - |\Sigma_{B_c}(B^*D) + \Sigma_{B_c}(BD^*)|(\kappa^{*2} = m_{B_c}^{*2}). \quad (2.64)$$

When we consider each loop contribution  $\Sigma_{B_c} = \Sigma(B^*D) + \Sigma(BD^*)$ ,  $m^0$  is a different value from that it is calculated in a situation considering only one loop.

In other words  $m^0(B^*D + BD^*) \neq m^0(B^*D)$ ,  $m^0(B^*D + BD^*) \neq m^0(BD^*)$  and nor  $m^0(B^*D + BD^*) \neq m^0(B^*D) + m^0(BD^*)$ . Thus, one should not compare directly the each loop contribution when the in-medium mass shift will be presented later.

From each self-energy contribution, one can only know which self-energy contribution is more dominant for the in-medium mass shift.

Each contribution reflects the mass reduction "effectiveness" for the total in-medium mass shift.

# Chapter 3

## Results

### 3.1 $B_c$ and $B_c^*$ meson results

Before presenting the numerical results (our predictions), it should be commented that, a phenomenological vertex form factor is used for each interaction vertex to tame the divergent loop integral appearing in the self-energy calculation. More about the regularization and the methods can be found in Ref. [84, 85, 86, 87].

For the  $B_c$  pseudoscalar meson we use the following form factors

$$\begin{aligned} u_{B^*DB^*}(\vec{q}^2) &= \left( \frac{\Lambda_{B^*D}^2 + m_{B_c}^2}{\Lambda_{B^*D}^2 + 4\omega_{B^*}^2(\vec{q}^2)} \right)^2, & u_{B^*DD}(\vec{q}^2) &= \left( \frac{\Lambda_{B^*D}^2 + m_{B_c}^2}{\Lambda_{B^*D}^2 + 4\omega_D^2(\vec{q}^2)} \right)^2, \\ u_{BD^*D^*}(\vec{q}^2) &= \left( \frac{\Lambda_{BD^*}^2 + m_{B_c}^2}{\Lambda_{BD^*}^2 + 4\omega_{D^*}^2(\vec{q}^2)} \right)^2, & u_{BD^*B}(\vec{q}^2) &= \left( \frac{\Lambda_{BD^*}^2 + m_{B_c}^2}{\Lambda_{BD^*}^2 + 4\omega_B^2(\vec{q}^2)} \right)^2. \end{aligned}$$

And for the  $B_c^*$  vector meson we use:

$$\begin{aligned} u_{BDB}(\vec{q}^2) &= \left( \frac{\Lambda_{BD}^2 + m_{B_c^*}^2}{\Lambda_{BD}^2 + 4\omega_B^2(\vec{q}^2)} \right)^2, \\ u_{BDD}(\vec{q}^2) &= \left( \frac{\Lambda_{BD}^2 + m_{B_c^*}^2}{\Lambda_{BD}^2 + 4\omega_D^2(\vec{q}^2)} \right)^2. \end{aligned}$$

In general, form factors are used to phenomenologically describe the finite size effect of particles and their interaction ranges or effectiveness. Thus, the form factors are necessary to include the effects of the finite sizes of the mesons and the overlapping regions associated with the interaction vertices. For this work we use dipole form factor which was well successful in previous works [72, 73, 74, 75, 76, 77].

The form factors contain the cutoff parameters, denoted by  $\Lambda_{B^*D}$ ,  $\Lambda_{BD^*}$  and  $\Lambda_{BD}$  which play non-negligible role to regularize the divergent integral and to get the final results. Note that, we will use,  $\Lambda_{B^*D} = \Lambda_{BD^*} = \Lambda_{BD} \equiv \Lambda$  hereafter. The value can introduce systematic uncertainties, and different physical processes might require different cutoff mass values, and possibly different form factors. For all the mesons studied in this thesis we use five different cutoff values varying  $\Lambda = 2000, 3000, 4000, 5000, 6000$  MeV. More details on the form factors can be seen in Refs. [48, 49, 52].

In Figs. 3.1, we show respectively the mass and mass shift of  $B_c$  meson in symmetric nuclear matter, varying five different values of the cutoff ( $\Lambda = 2000, 3000, 4000, 5000, 6000$  MeV). In the figures,  $\Delta m$  is the mass shift ( $\Delta m = m^* - m$ ) and  $\rho_0 = 0.15 \text{ fm}^{-3}$  is the symmetric nuclear matter saturation density and  $\rho_B$  is the baryon density.

The physical free space masses used in calculation are  $m_{B_c} = 6274.5$  MeV,  $m_{B_c^*} = 6333.0$  MeV, and since there is no experimental data of  $B_c^*$  we use an average value of those presented in Ref. [50]. (See Table 1.6)

Note that, in Fig. 3.4,  $B_c$  total mass shift is provided by the sum of the two loop contributions as shown in Fig. 2.3 (top panel).

In Fig. 3.2 it is explicitly shown the density dependence of self-energy for each loop and its total, besides that, it is shown the density dependence of total self-energy for each cutoff value separately for the  $B_c$  meson.

These self-energy results show negative shift in effective masses (or attractive Lorentz scalar potentials), what can be interpreted as attractive Lorentz scalar potentials provided by the effects of the nuclear medium [45]. (Note that, as already commented, in quantum mechanics, the second order perturbation always gives the negative contribution for the energy, and one can understand based on this picture when the intermediate state energies are more than that of the initial and final states.)

The interesting question that arises is whether or not this attraction is strong enough to bind these mesons to a nucleus. Thus, the next step should be to look for nucleus bound states.

We remind that, for each case in graphs shown in Fig. 3.1,  $m^0$  is determined to reproduce the physical mass  $m_{B_c}$  in free space.

As we noted after Eqs. (2.6)-(2.8) as well as Eq. (2.49), one should be careful in comparing each loop contribution in Table 3.1. For each loop contribution  $B^*D, BD^*$

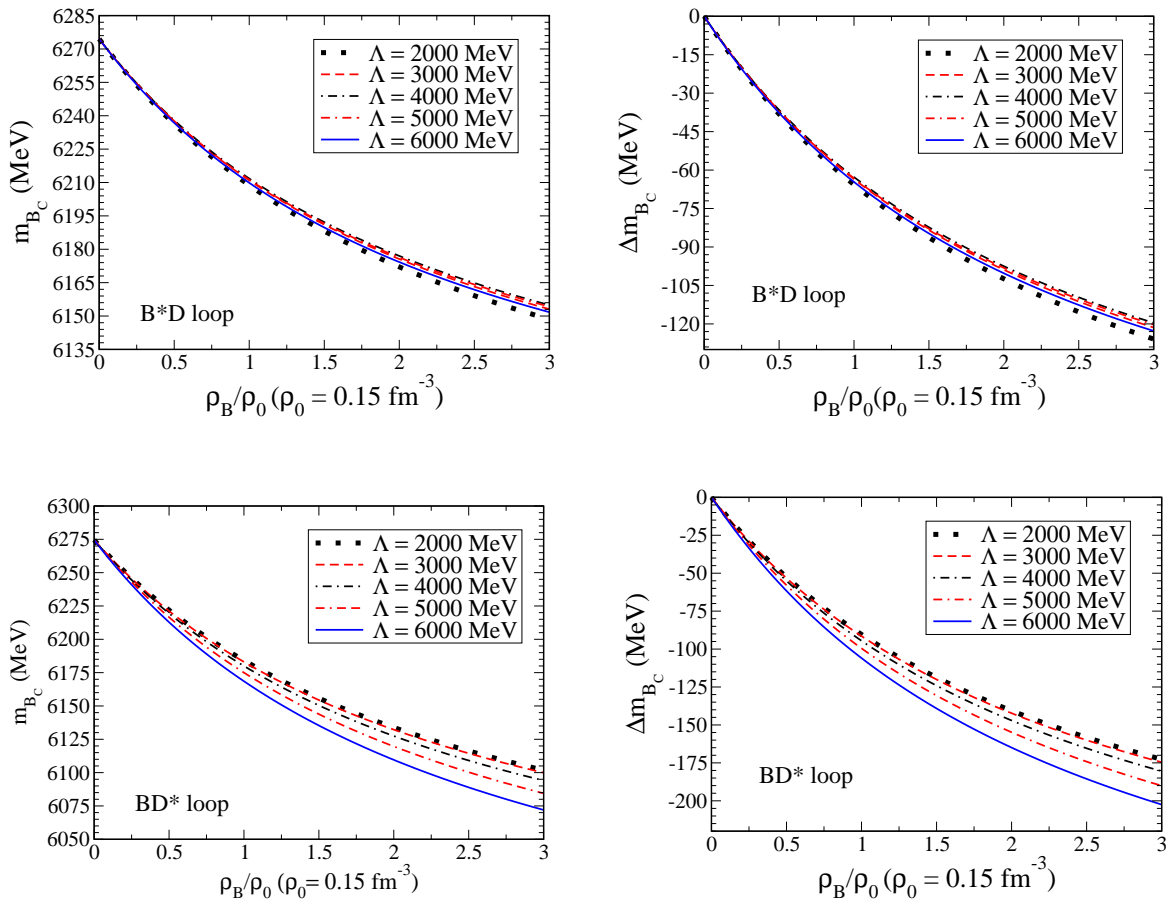


Figure 3.1: In-medium mass (left panel) and mass shift (right panel) of  $B_c$  meson (i) only including the  $B^*D$  loop (top) and (ii) only including the  $BD^*$ .  $\rho_0 = 0.15 \text{ fm}^{-3}$  is the symmetric nuclear matter saturation density and  $\rho_B$  is the baryon density.

and  $B^*D + BD^*$ ,  $m^0$  is fixed as  $m^0(B^*D)$ ,  $m^0(BD^*)$  and  $m^0(B^*D + BD^*)$  respectively, to reproduce each case the physical free mass of  $m_{B_c}$ . We can see more details in Table 3.2.

By Table 3.1, we can conclude that, for the total mass shift including the  $B^*D + BD^*$  loops, the  $BD^*$  loop is more dominant than the  $B^*D$  loop. This indeed shows that very naive expectation by comparing the total mass values *does not* work. This may also be caused by the fact that the total mass values for these two loops are very close.

A possible explanation is as follows. Looking at Eq. (3.2) for the  $B^*D$  loop, it contains  $B^*$  vector meson propagator, which results in the expression Eq. (2.50). For the  $BD^*$  loop instead, one may replace  $m_B^* \rightarrow m_D^*$  in Eq. (2.50). Since  $m_{B^*} - m_B \simeq 45 \text{ MeV} \ll m_{B^*} - m_{D^*} \simeq 2300 \text{ MeV}$  and  $m_{D^*} - m_D \simeq 140 \text{ MeV} \ll m_{B^*} - m_{D^*} \simeq 2300 \text{ MeV}$ , thus, even in nuclear medium the  $B^*$  and  $D^*$  role change is expected to give significant effect of the  $D^*$  meson propagator.

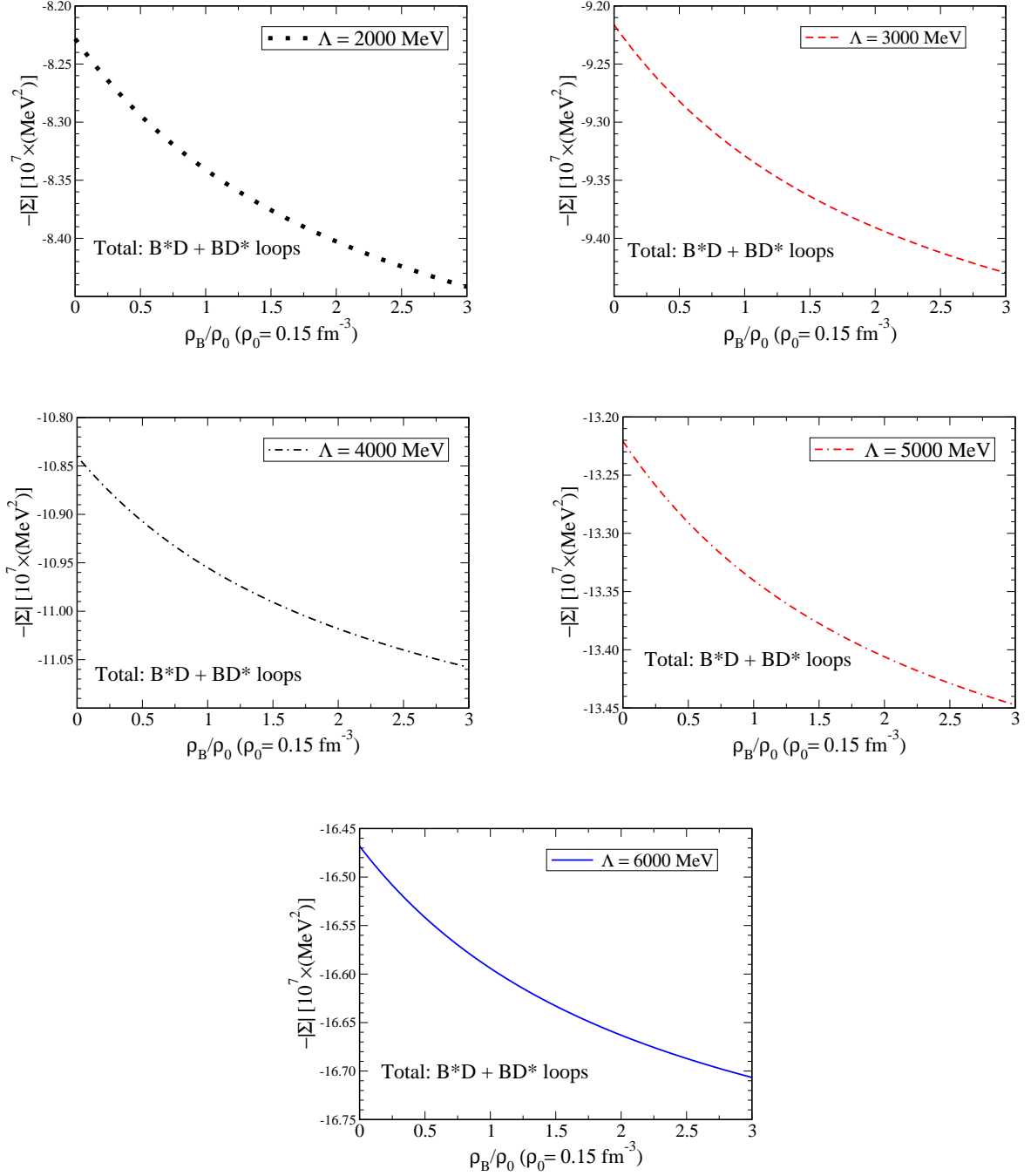


Figure 3.2:  $B_c$  self-energy values considering total two possible loops. Each figure shows the self-energy for total loop considering both loops for a different cutoff value.  $\rho_0 = 0.15 \text{ fm}^{-3}$  is the symmetric nuclear matter saturation density and  $\rho_B$  is the baryon density.

Thus, the conclusion is that the  $D^*$  meson propagator, in particular the numerator which represents the spin-1 nature, is much more effectively contributing to the self-energy integral than that of the  $B^*$ .

Note that in Fig. 3.3 we present the self-energy decomposition of meson  $B_c$ . It

Table 3.1:  $\Delta m$  for  $B_c$  meson at  $3\rho_0$  for all the five cutoff value ( $\Lambda = 2000, 3000, 4000, 5000, 6000$  MeV).

$\Lambda$ (MeV)	$B^*D$ (MeV)	$BD^*$ (MeV)	$B^*D + BD^*$ (MeV)
2000	-125.9	-172.7	-172.4
3000	-121.4	-174.6	-172.5
4000	-119.6	-180.4	-176.1
5000	-120.3	-190.0	-183.2
6000	-122.8	-202.5	-192.9

Table 3.2:  $m^0$  considering  $B^*D$  loop,  $BD^*$  loop and total  $B^*D + BD^*$ .

$\Lambda$ (MeV)	$m^0$ ( $B^*D$ ) (MeV)	$m^0$ ( $BD^*$ ) (MeV)	$m^0$ ( $B^*D + BD^*$ ) (MeV)
2000	7906.1	9925.4	11029.6
3000	8032.6	10313.9	11468.7
4000	8249.0	10913.0	12156.0
5000	8561.5	11732.3	13098.8
6000	8968.6	12766.7	14284.6

seems that the density dependence is small but it is due to the vertical scale.

Table 3.3:  $\Delta m$  in medium for  $B_c^*$  meson at  $3\rho_0$  for all the five cutoff value ( $\Lambda = 2000, 3000, 4000, 5000, 6000$  MeV).

$\Lambda$ (MeV)	$BD$ (MeV)
2000	-29.4
3000	-30.1
4000	-31.9
5000	-34.9
6000	-38.8

Figures 3.5 and 3.6 show the decomposition of  $B_c^*$  meson self-energy and its mass

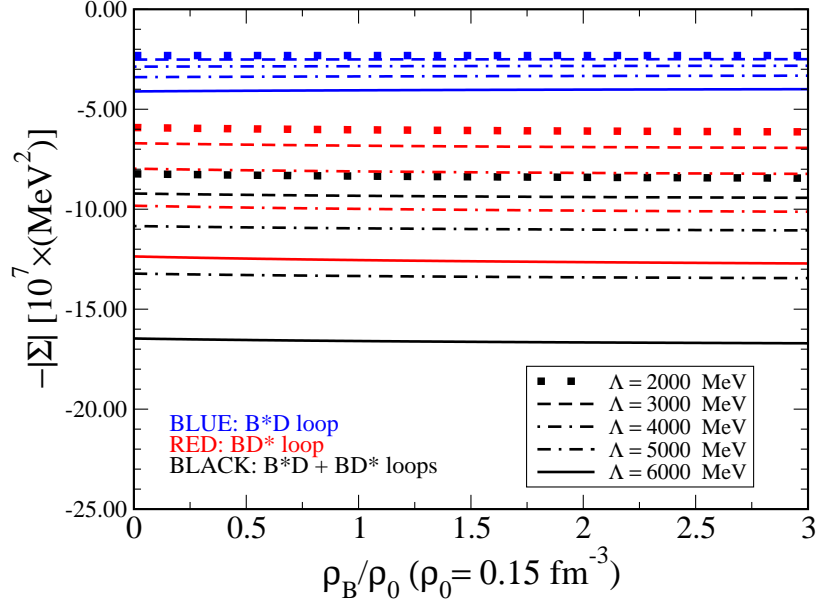


Figure 3.3: Decomposition of the  $B_c$  meson total self-energy for different cutoff mass values.

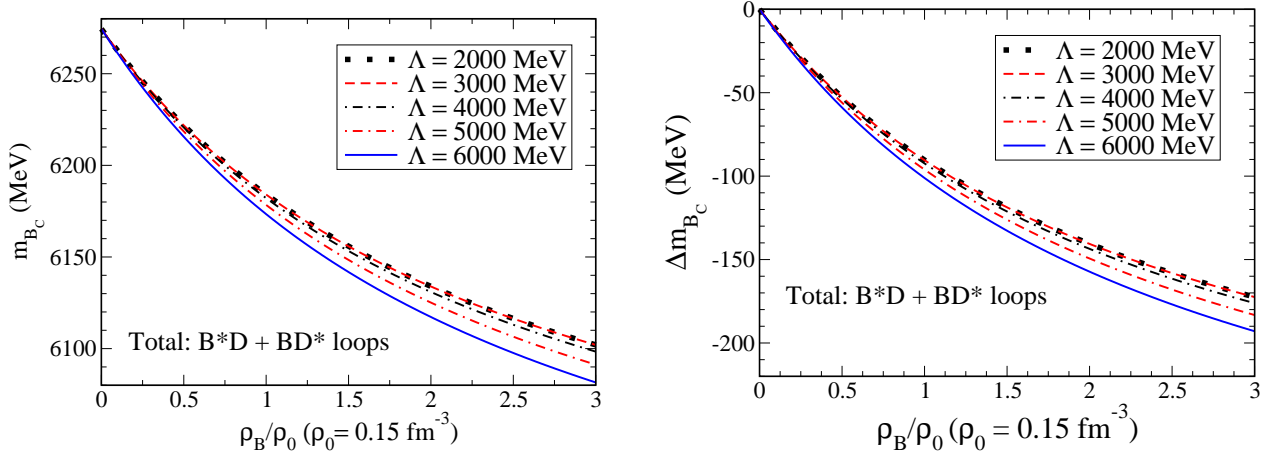


Figure 3.4:  $B_c$  in-medium mass (left) and mass shift (right).  $\rho_0 = 0.15 \text{ fm}^{-3}$  is the symmetric nuclear matter saturation density and  $\rho_B$  is the baryon density.

and mass-shift respectively.

Table 3.4 shows how  $m^0$  value varies against the cut-off value, and Table 3.3 shows the mass shift of  $B_c^*$  for the each cut-off value.

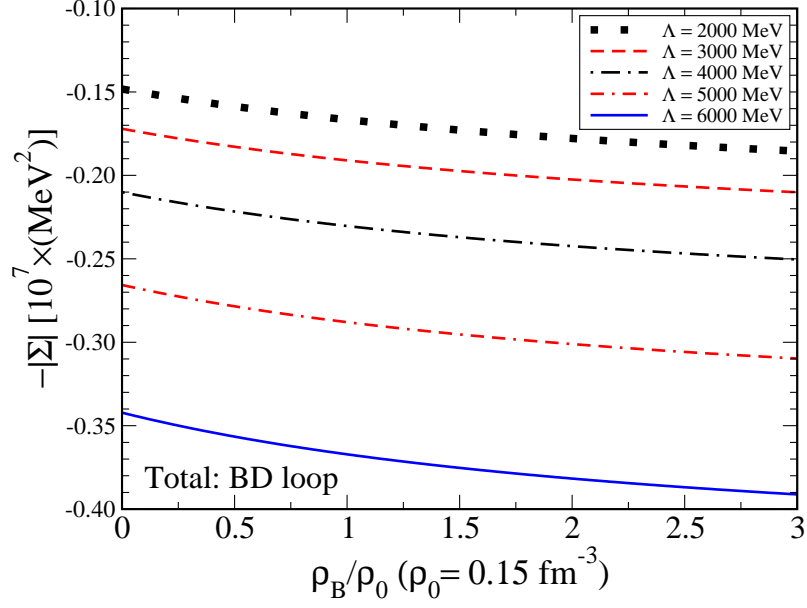


Figure 3.5:  $B_c^*$  self-energies for different cutoff mass values.

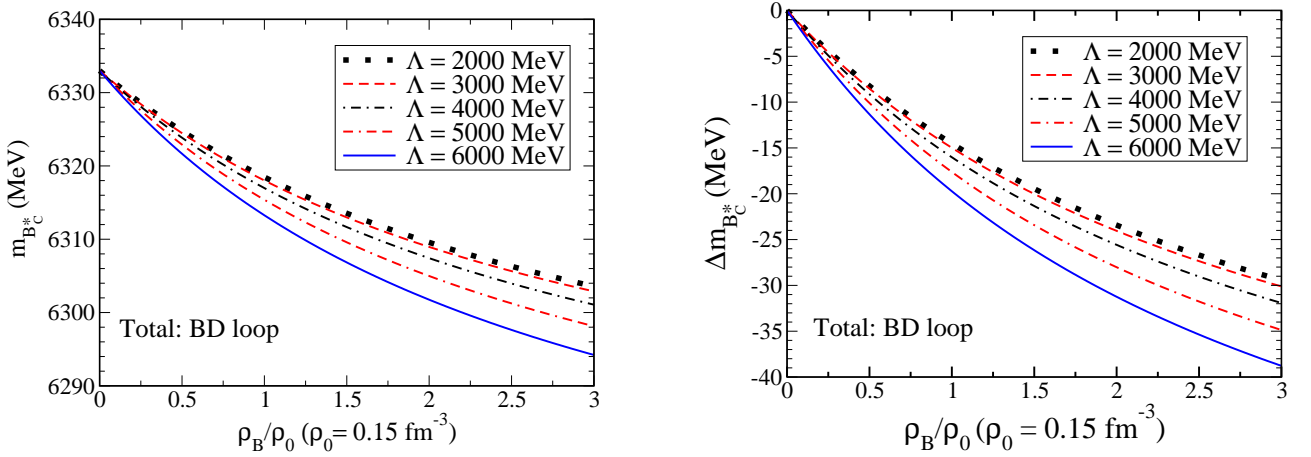


Figure 3.6:  $B_c^*$  in-medium mass (left) and mass shift (right).  $\rho_0 = 0.15 \text{ fm}^{-3}$  is the symmetric nuclear matter saturation density and  $\rho_B$  is the baryon density.

We also study the in-medium mass shift of the heavy-strange mesons  $B_s, B_s^*, D_s$  and  $D_s^*$  using the same method used for  $B_c$  and  $B_c^*$ .

The free space mass of each meson is,  $m_{B_s} = 5366.9 \text{ MeV}$ ,  $m_{B_s^*} = 5415.4 \text{ MeV}$ ,  $m_{D_s} = 1968.4 \text{ MeV}$  and  $m_{D_s^*} = 2112.2 \text{ MeV}$ .

Table 3.4:  $m^0$  considering  $BD$  loop.

$\Lambda$ (MeV)	$m^0$ ( $BD$ ) (MeV)
2000	6449.0
3000	6467.4
4000	6496.8
5000	6539.4
6000	6597.7

### 3.2 $B_s^0$ and $B_s^*$ meson results

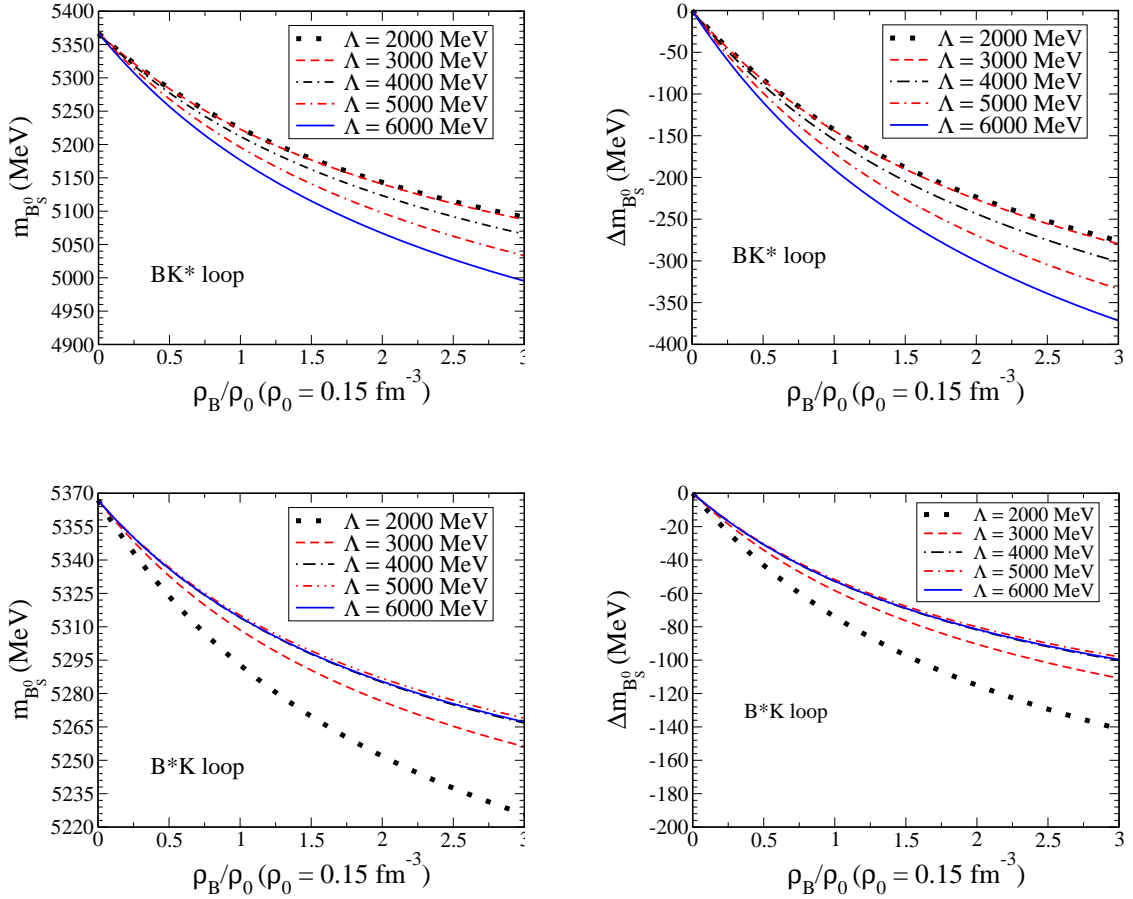


Figure 3.7: In-medium mass (left panel) and mass shift (right panel) of  $B_s^0$  meson (i) only including the  $BK^*$  loop (top) and (ii) only including the  $B^*K$ .  $\rho_0 = 0.15 \text{ fm}^{-3}$  is the symmetric nuclear matter saturation density and  $\rho_B$  is the baryon density.

Fig. 3.7 shows the mass and the mass shift of  $B_s^0$  where we can check that  $B_s^0$

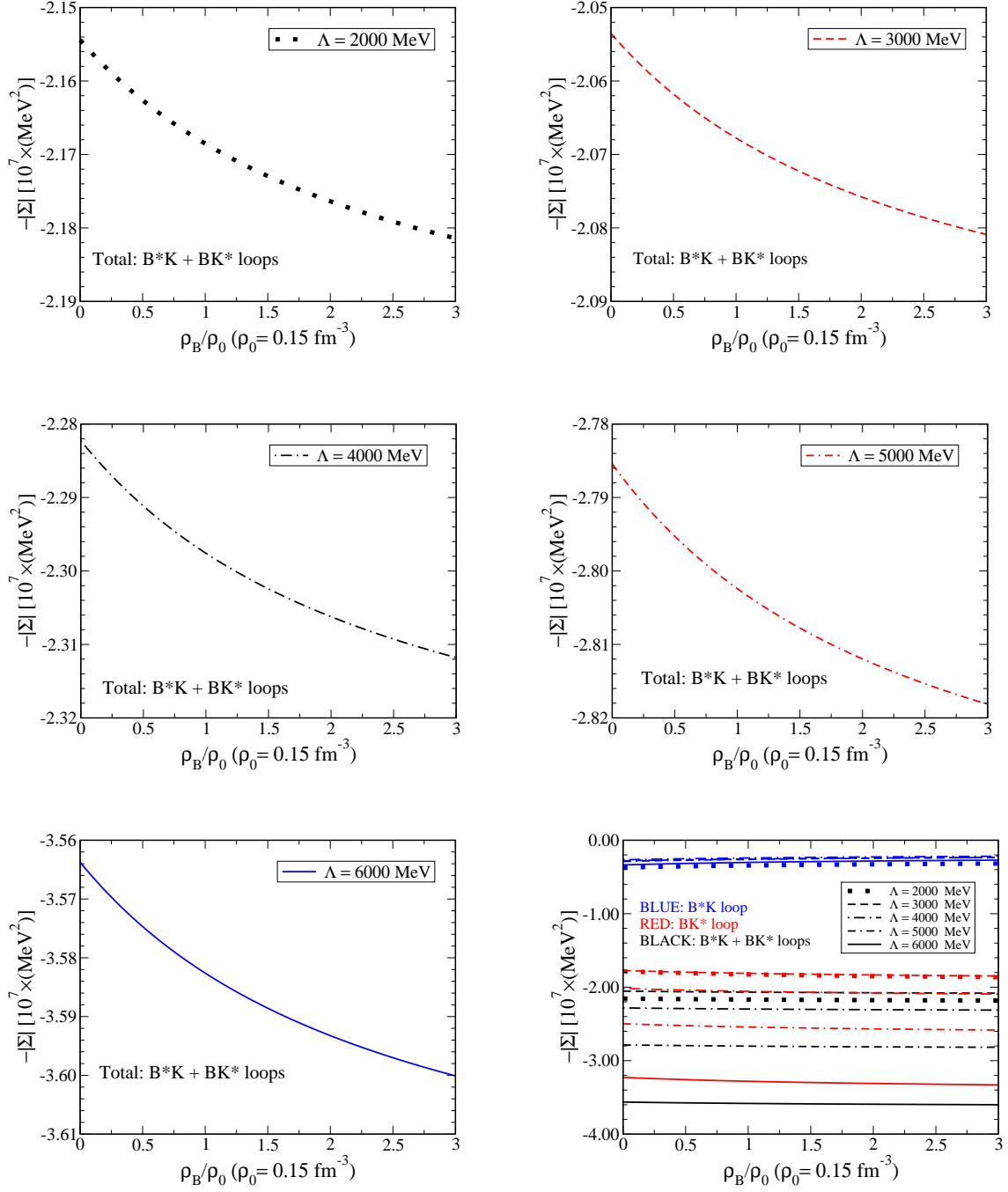


Figure 3.8:  $B_s^0$  self-energy values. Each panel shows the self-energy for total loop contribution including the both loops but for a different cutoff value. The figure in the bottom-right panel shows a comparison among all of them including the total and the two possible loops separately.

shares a similarity with  $B_c$ , since  $B^*K$  loop gives smaller contribution than  $BK^*$  for this meson total self-energy. In the same way, a possible explanation is that the lighter vector meson (excited)  $K^*$  propagator gives this result. Figure 3.8 explicitly shows the

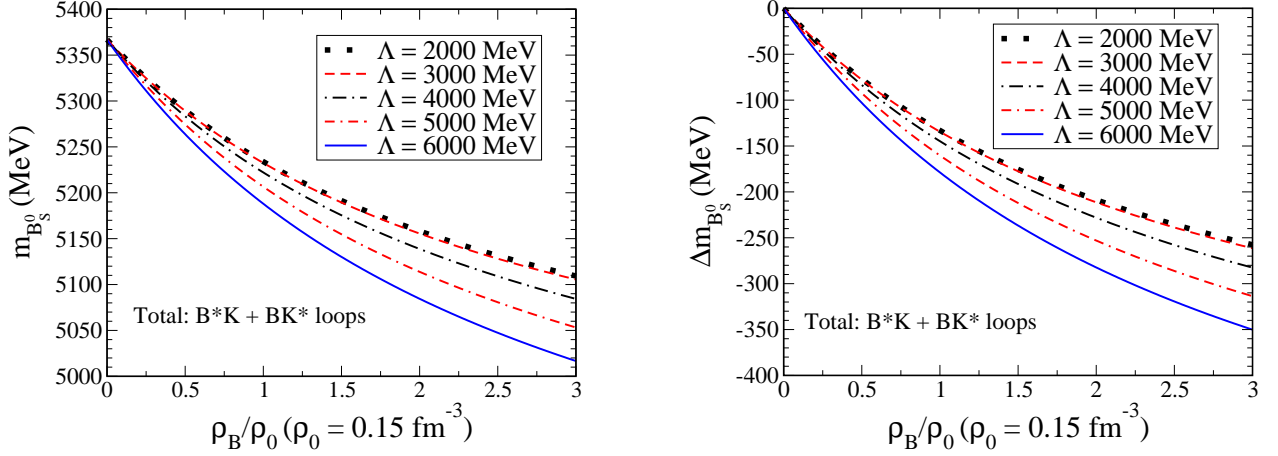


Figure 3.9:  $B_s^0$  in-medium mass (left) and mass shift (right).  $\rho_0 = 0.15 \text{ fm}^{-3}$  is the symmetric nuclear matter saturation density and  $\rho_B$  is the baryon density.

Table 3.5:  $\Delta m$  in medium for  $B_s^0$  meson at  $3\rho_0$  for all the five cutoff value ( $\Lambda = 2000, 3000, 4000, 5000, 6000 \text{ MeV}$ ).

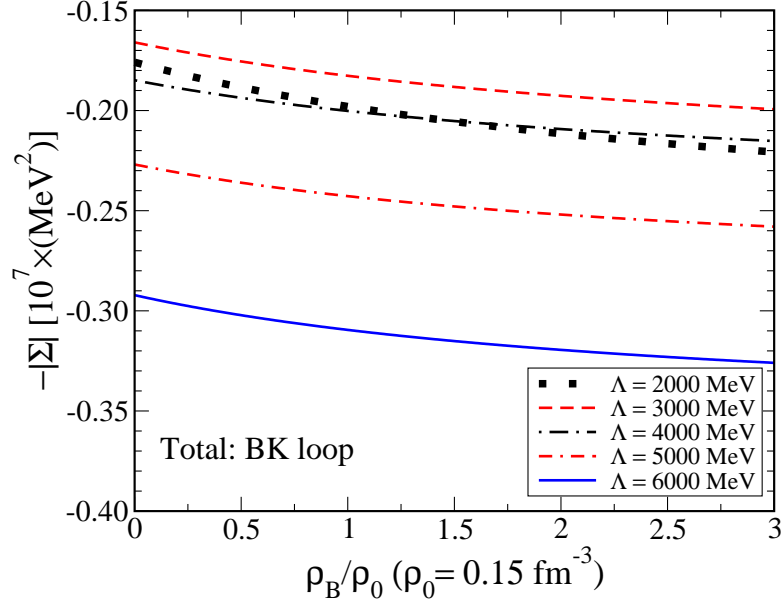
$\Lambda$ (MeV)	$B^*K$ (MeV)	$BK^*$ (MeV)	$B^*K + BK^*$ (MeV)
2000	-141.1	-275.8	-257.6
3000	-110.8	-279.5	-261.4
4000	-100.2	-301.2	-282.5
5000	-98.0	-333.5	-313.6
6000	-99.7	-371.5	-350.2

self-energy values for each loop and its total. In Fig. 3.9 we show the mass (left) and mass shift (right) of  $B_s^0$  considering total loop contribution, and in Table. 3.5 the mass shift values of each loop for each cut-off value at  $3\rho_0$ . Table 3.6 shows the  $m_0$  for each cut-off value.

Fig. 3.11 shows the results obtained for the mass (left), mass shift (right) and Fig. 3.10 shows the self-energy for each calculated cut-off value of the vector meson  $B_s^*$  and Table 3.7 gives more details about the mass shift in each cut off value. Table 3.8 shows  $m^0$  for each calculated cut-off value of the vector meson  $B_s^*$ .

Table 3.6:  $m^0$  considering  $B^*K$  loop  $BK^*$  loop and total  $B^*K + BK^*$ .

$\Lambda$ (MeV)	$m^0 (B^*K)$ (MeV)	$m^0 (BK^*)$ (MeV)	$m^0 (B^*K + BK^*)$ (MeV)
2000	8114.6	14394.5	15628.3
3000	7536.4	14358.3	15302.1
4000	7441.7	15180.7	16032.1
5000	7592.3	16688.6	17531.3
6000	7899.3	18750.5	19625.9

Figure 3.10:  $B_s^*$  self-energies for different cutoff mass values.

### 3.3 $D_s$ and $D_s^*$ meson results

Figures 3.15 and 3.16 show the results for the self-energy the in-medium mass (left) and mass shift (right) of the vector meson  $D_s^*$ . Table 3.11 shows a detailed analyses of its mass shift value for each cut-off value. Table 3.12 shows  $m_0$  value for each cut-off value.

After presenting all the obtained results we summarize in Table 3.13 the density

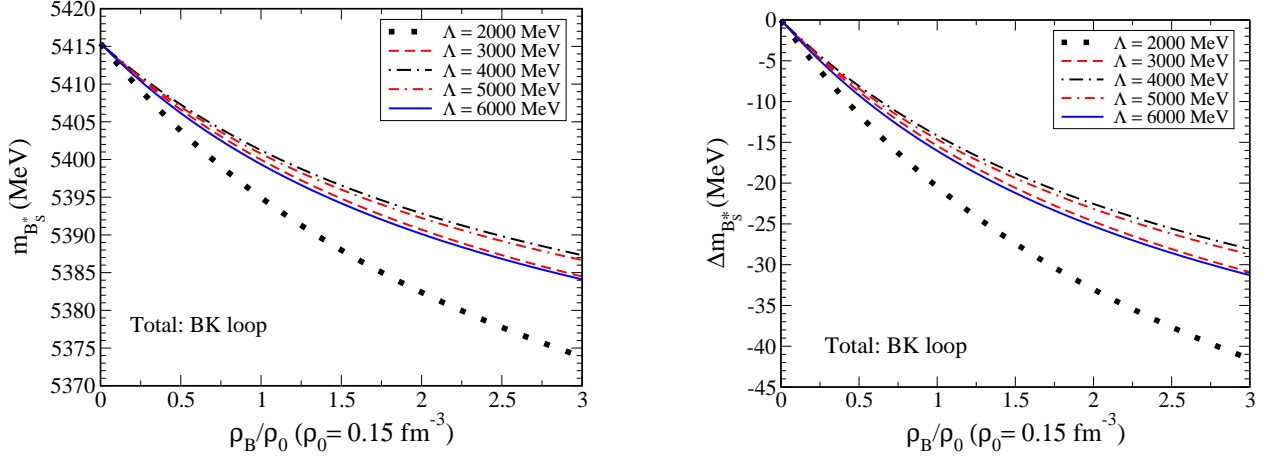


Figure 3.11:  $B_s^*$  in-medium mass (left) and mass shift (right).

Table 3.7:  $\Delta m$  in medium for  $B_s^*$  meson at  $3\rho_0$  for all the five cutoff value ( $\Lambda = 2000, 3000, 4000, 5000, 6000$  MeV).

$\Lambda$ (MeV)	$BK$ (MeV)
2000	-41.6
3000	-30.9
4000	-28.1
5000	-28.7
6000	-31.3

Table 3.8:  $m^0$  considering  $BK$  loop.

$\Lambda$ (MeV)	$m^0$ ( $BK$ ) (MeV)
2000	5575.42
3000	5566.5
4000	5583.5
5000	5621.0
6000	5678.8

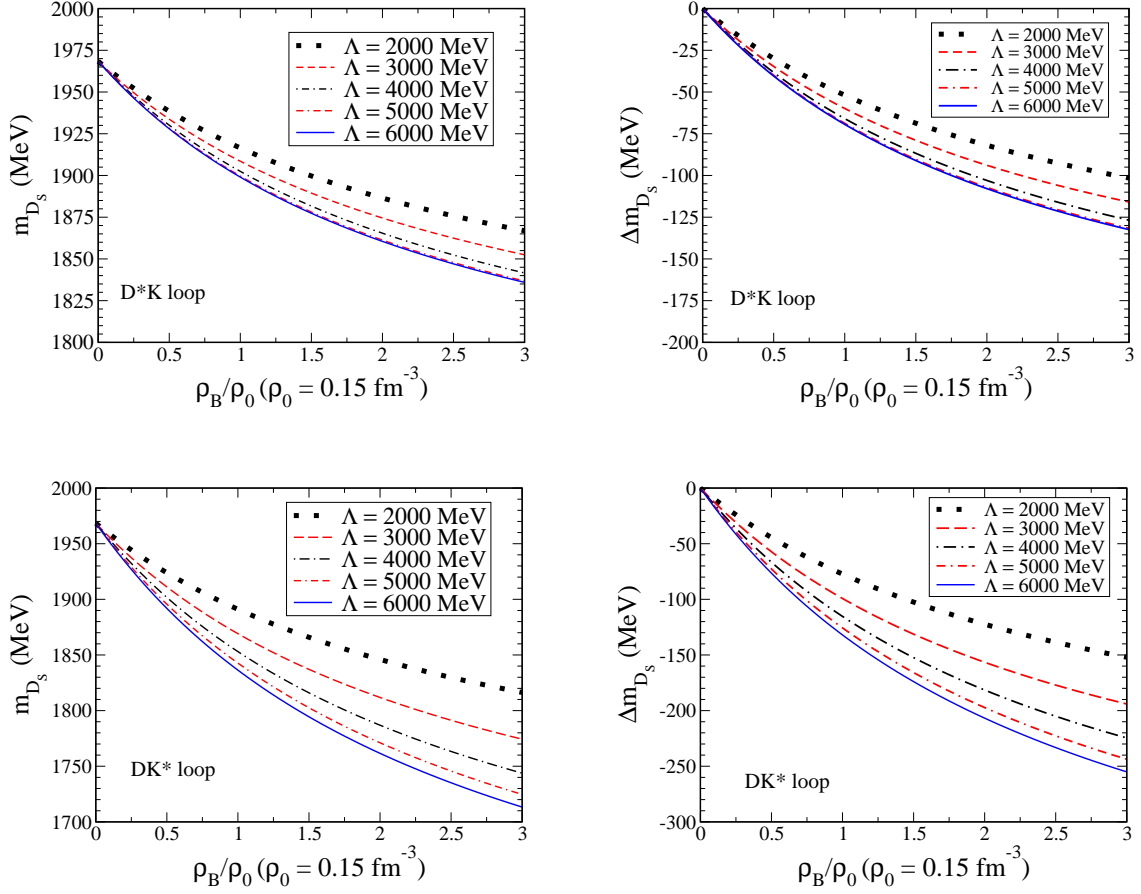


Figure 3.12: In-medium mass (left panel) and mass shift (right panel) of  $D_s$  meson (i) only including the  $D^*K$  loop (top) and (ii) only including the  $DK^*$ .  $\rho_0 = 0.15 \text{ fm}^{-3}$  is the symmetric nuclear matter saturation density and  $\rho_B$  is the baryon density.

Table 3.9:  $\Delta m$  for  $D_s$  meson at  $3\rho_0$  for all the five cutoff value ( $\Lambda = 2000, 3000, 4000, 5000, 6000 \text{ MeV}$ ).

$\Lambda$ (MeV)	$D^*K$ (MeV)	$DK^*$ (MeV)	$D^*K + DK^*$ (MeV)
2000	-101.5	-152.0	-152.2
3000	-115.9	-194.0	-183.9
4000	-126.8	-224.6	207.3
5000	-131.7	-243.7	-221.8
6000	-132.5	-255.1	-230.3

dependence of the in-medium mass (where  $\rho_0 = 0.15 \text{ fm}^{-3}$  is the nuclear matter saturation density and  $\rho_B$  is the baryon density). We have used the same parameters as those

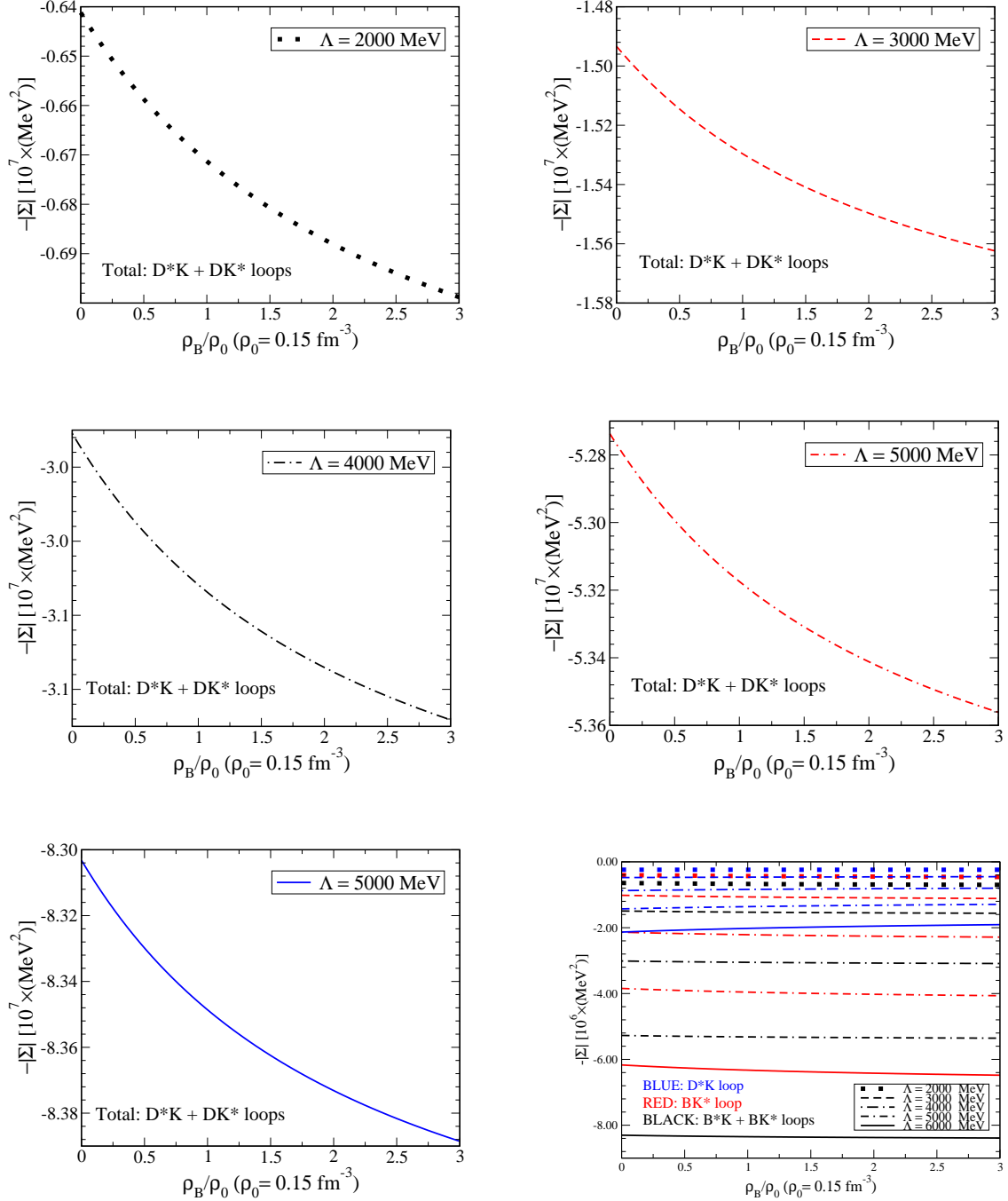


Figure 3.13:  $D_s$  self-energy values. Each panel shows the self-energy for the total loop contribution from both loops but a different cutoff value, and the figure in the right-bottom panel shows a comparison among all of them including the total and two different each possible loop.

previously used in Ref. [40] but now we include the values obtained in this work. (For  $m_{B_c^*}$  at  $\rho_B = 0$  value we extract the average value from [50].)

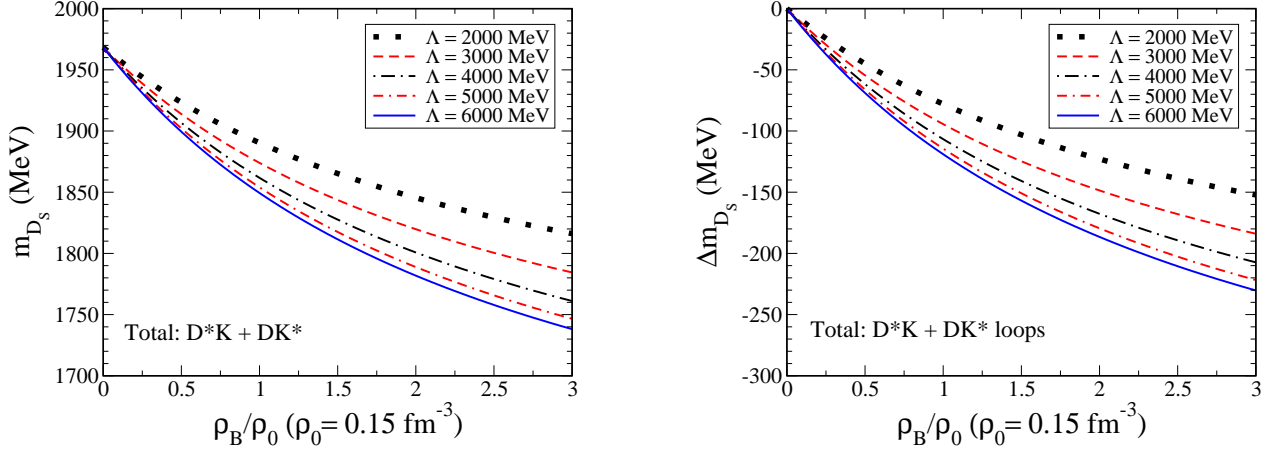


Figure 3.14:  $D_s$  in-medium mass (left) and mass shift (right).  $\rho_0 = 0.15 \text{ fm}^{-3}$  is the symmetric nuclear matter saturation density and  $\rho_B$  is the baryon density.

Table 3.10:  $m^0$  considering  $D^*K$  loop  $DK^*$  loop and total  $D^*K + DK^*$ .

$\Lambda$ (MeV)	$m^0 (D^*K)$ (MeV)	$m^0 (DK^*)$ (MeV)	$m^0 (D^*K + DK^*)$ (MeV)
2000	2503.1	2809.9	3207.3
3000	2940.5	3746.6	4336.8
4000	3551.1	5024.7	5829.5
5000	4262.1	6505.5	7524.1
6000	5021.3	8097.4	9322.4

Table 3.11:  $\Delta m$  for  $D_s^*$  meson at  $3\rho_0$  for all the five cutoff value ( $\Lambda = 2000, 3000, 4000, 5000, 6000$  MeV).

$\Lambda$ (MeV)	$DK$ (MeV)
2000	-44.6
3000	-57.2
4000	-72.9
5000	-88.4
6000	-102.4

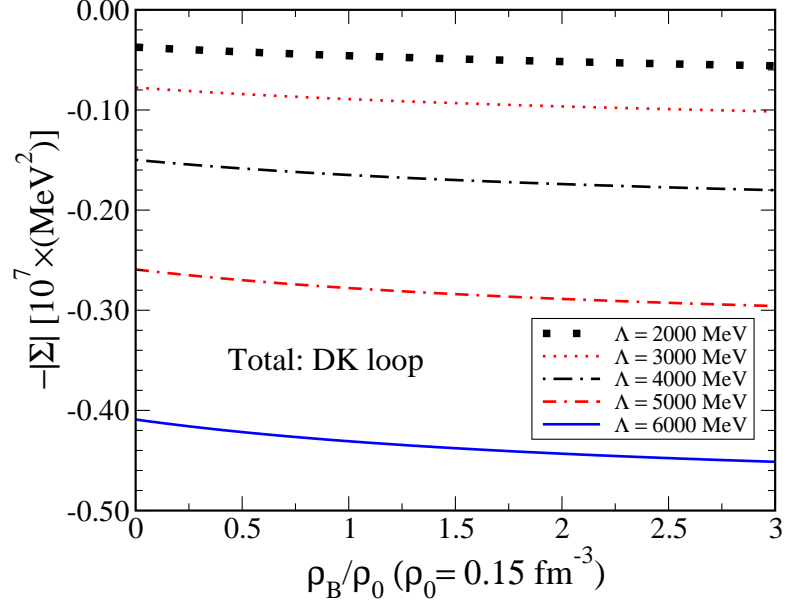


Figure 3.15:  $D_s^*$  self-energies for different cutoff mass values.

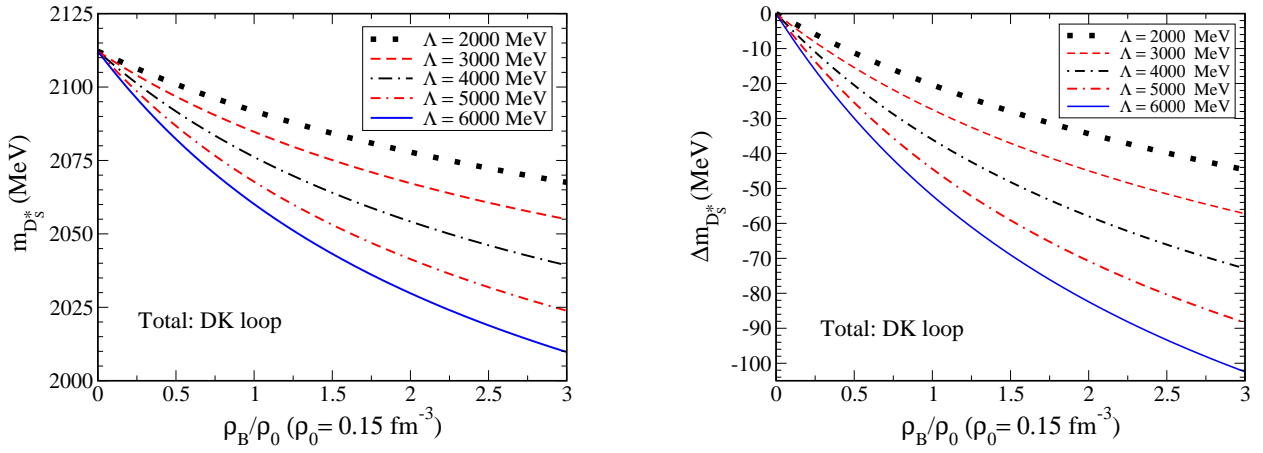


Figure 3.16:  $D_s^*$  in-medium mass (left) and mass shift (right).

Table 3.12:  $m^0$  considering  $DK$  loop.

$\Lambda$ (MeV)	$m^0$ ( $DK$ ) (MeV)
2000	2198.66
3000	2288.6
4000	2441.2
5000	2656.0
6000	2924.4

Table 3.13: Density dependence of meson (effective) masses in MeV calculate in the QMC model with  $m_{u,d} = 5$  MeV,  $m_s = 250$  MeV,  $m_c = 1270$  MeV and  $m_b = 4200$  MeV. ( $\rho_0 = 0.15 \text{ fm}^{-3}$  below.)

	$\rho_B = 0$ (MeV)	$\rho_B = \rho_0$ (MeV)	$\rho_B = 2\rho_0$ (MeV)	$\rho_B = 3\rho_0$ (MeV)
$m_K$	493.7	430.5	393.6	369.0
$m_{K^*}$	893.9	831.9	797.2	775.0
$m_D$	1867.2	1805.2	1770.6	1748.4
$m_{D^*}$	2008.6	1946.9	1912.9	1891.2
$m_B$	5279.3	5218.2	5185.1	5164.4
$m_{B^*}$	5324.7	5263.7	5230.7	5210.2
$m_{B_c^+}$	6274.5	6184.1	6134.0	6102.1
$m_{B_c^*}$	6333.0	6318.5	6309.6	6303.6
$m_{B_s^0}$	5366.9	5233.8	5158.2	5109.3
$m_{B_s^*}$	5415.4	5394.9	5382.4	5373.8
$m_{D_s^\pm}$	1968.4	1890.4	1845.5	1816.2
$m_{D_s^{*\pm}}$	2112.2	2091.8	2077.8	2067.5

# Chapter 4

## Comparison with heavy quarkonia

As we previously mentioned, some of our interest in studying mesons  $B_c$  and  $B_c^*$  relies on the fact that they are composed of a bottom and a charm quarks. Then, we can very naively expect that they may present the properties and characteristics between the mesons composed of only by a pair of charm-anticharm and a pair of bottom-antibottom.

We have found that  $B_c^*$  mass shift lies in-between of the  $\Upsilon$  and  $J/\psi$  properties, however,  $B_c$  does not present such an expected simple characteristic. A more detailed comparison is shown in Fig. 4.1.

The  $B_c$  mass shift, however, presents a more negative shift than  $\eta_c$  and  $\eta_b$  when including the  $B^*D + BD^*$  (fig. 4.1). The same happens by including the  $BD^*$  loop, a less negative shift occur when including the  $B^*D$  loop, though (not explicitly shown in Fig. 4.1).

In Fig. 4.1,  $\eta_b$  self-energy includes only the  $BB^*$  loop contribution and its mass shift range from -75 to -82 MeV, for the cutoff  $\Lambda$  values of 2000, 3000, 4000, 5000 and 6000 MeV at  $\rho_0$ . For the  $\eta_c$  self-energy, it only includes the  $DD^*$  loop contribution and corresponds to the mass shift value range from -41.18 to -86.49 MeV, for the cutoff  $\Lambda_D$  values of 2000, 4000 and 6000 at  $\rho_0$ .

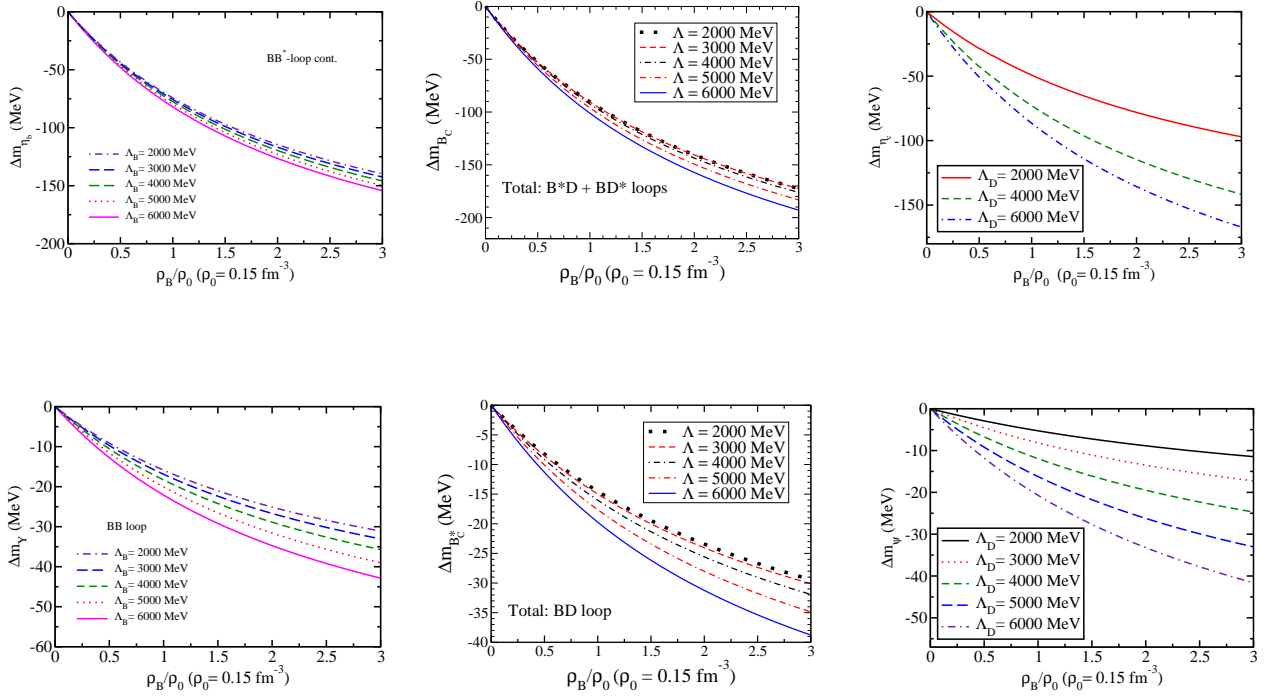


Figure 4.1: Comparison of the in medium mass shift of pseudoscalar (top) and vector (bottom) mesons,  $\eta_b$  (top-left),  $B_c$  (top-center)  $\eta_c$  (top-right)  $\Upsilon$  (bottom-left),  $B_c^*$  (bottom-center) and  $J/\Psi$  (bottom-right).  $\rho_0 = 0.15 \text{ fm}^{-3}$  is the symmetric nuclear matter saturation density and  $\rho_B$  is the baryon density.

# Chapter 5

## Conclusion

In this thesis, extending the previous works of  $J/\psi$ ,  $\eta_c$ ,  $\eta_b$  and  $\Upsilon$  mass shift in symmetric nuclear matter [45, 48, 49, 52], we have estimated, for the first time, the  $B_c$ ,  $B_c^*$ ,  $B_s$ ,  $B_s^*$ ,  $D_s$  and  $D_s^*$  meson mass shift in symmetric nuclear matter. We have estimated the meson self-energy loop contributions using an effective flavor SU(5) symmetry based Lagrangians with one universal coupling constant to be able to relate various coupling constants appearing in the effective Lagrangian density for each meson. The value for the universal coupling constant is calculated from the experimental data with the vector meson dominance (VMD) model, namely by the data  $\Upsilon \rightarrow e^+e^-$ . The in medium masses of mesons  $B$ ,  $B^*$ ,  $D$ ,  $D^*$ ,  $K$ ,  $K^*$  were calculated using the quark-meson coupling model.

For the studies of  $\Upsilon$  and  $\eta_b$  in-medium mass shift [49], we have used a similar approach using an effective flavor SU(5) symmetry based Lagrangian, and the anomalous coupling one, but in this work we have not included the latter.

For the  $B_c$  pseudoscalar meson, instead, we have to include two possible loops  $BD^*$  and  $B^*D$  for the self-energy processes, and no anomalous coupling loops. Note that, these two loop contributions are based on the same footing as those for the  $\eta_c$  and  $\eta_b$  (PPV: pseudoscalar-pseudoscalar-vector) coupling from the same SU(5) symmetric Lagrangian.

We have followed the same procedure for the pseudoscalar meson  $B_s$ , considering only the first order loops  $BK^*$  and  $B^*K$ , and for  $D_s$ , including the first order, the loops  $DK^*$  and  $D^*K$ .

Since  $B_c^*$  is a vector meson and our effective Lagrangians are obtained by the PPV interaction, the intermediate states is composed by  $BD$  loop, and, for this same reason  $B_s^*$  and  $D_s^*$  the included loops for each of them are respectively  $BK$  and  $DK$ .

For each meson we have presented results for the in-medium masses, mass shift (scalar potential) and self-energy, varying the cutoffs ( $\Lambda = 2000, 3000, 4000, 5000, 6000$  MeV), following our previous works and we have used a dipole form factor.

Our results show that  $BD^*$  loop self-energy gives a larger contribution than that of the  $B^*D$ , and this disagrees with our initial very naive expectation based on non-relativistic quantum mechanics second-order perturbation theory. It implies that the lighter vector meson  $D^*$  than  $B^*$  in the self-energy loop gives more effective contribution due to the vector meson propagator Lorentz structure.

We have found that the  $B_c$  meson mass shift at  $3\rho_0$  varies from  $-152.2$  MeV ( $\Lambda = 2000$  MeV) to  $-230.3$  MeV ( $\Lambda = 6000$  MeV).

While the results of mass shift for  $B_c^*$  varies from  $-29.4$  MeV ( $\Lambda = 2000$  MeV) to  $-38.8$  MeV ( $\Lambda = 6000$  MeV).

Our results can be summarized as  $|\Delta m_{\eta_c}| < |\Delta m_{\eta_b}| < |\Delta m_{B_c}|$  and  $|\Delta m_{J/\psi}| < |\Delta m_{B_c^*}| < |\Delta m_{\Upsilon}|$ .

Besides that, we have also studied and presented the in-medium masses, mass shift and their density dependence for the mesons,  $B_s, B_s^*, D_s$  and  $D_s^*$ .

Based on the studies made in this thesis, a few future extended studies are planned: (i) Study of meson-nucleus bound states for some selected mesons in  $B_c, B_c^*, B_s, B_s^*, D_s$  and  $D_s^*$ , (ii) study of the in-medium properties of these mesons, such as weak-interaction properties, electromagnetic properties, and (iii) reactions involving these mesons in (heavy mass) nucleus.

# Chapter 6

## Appendix A

### 6.1 Poles in integration

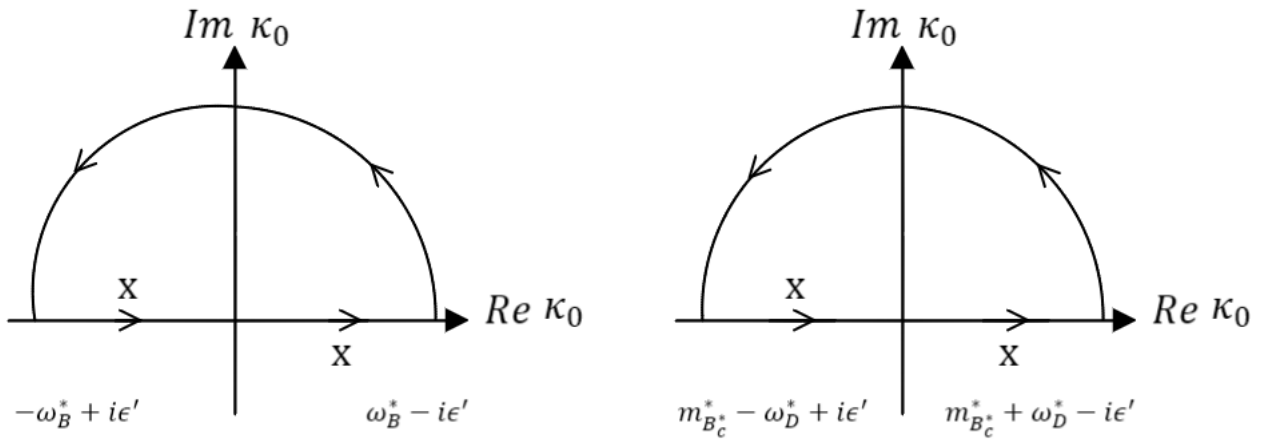


Figure 6.1: Integration of  $\kappa_0$  in the complex plane.

In this appendix we show how we perform the complex integration of  $\kappa_0$  in Eqs. (2.57) and (2.58) by showing the corresponding figures in Fig. 6.1, left and right pannels, respectively.

For Eqs. (2.57) and (2.58) the integration contains poles in  $\kappa_0^2 = \vec{\kappa}^2 + m^2$ , and this can be handled by the standard Cauchy integral.

With  $\kappa_0 + V \rightarrow \kappa_0$  denoting the vector potential shifted, or changing the integral variables. By going into the complex plane considering  $\kappa_0$  as a complex variable we can take the paths shown in 6.1.

Our choice should be the one that the integral under the circular area goes to zero when the radius  $R$  goes to infinite.

For the left hand side diagram in Fig 6.1 we proceed,

$$\kappa^2 - m_B^{*2} + i\epsilon = k_0^2 - (\vec{\kappa}^2 + m_B^{*2}) + i\epsilon = 0,$$

$$(\vec{\kappa}^2 + m_B^{*2}) \equiv \omega_B^{*2},$$

$$\omega_B^* = \sqrt{\vec{\kappa}^2 + m_B^{*2}},$$

$$\begin{aligned} \kappa_0 &= \pm \sqrt{\omega_B^{*2} - i\epsilon}, \\ &= \pm \omega_B^* \mp i\epsilon, \end{aligned}$$

$$k_0 = -\omega_B^*. \quad (6.1)$$

Similarly, for the right hand side diagram in Fig 6.1 we proceed,

$$(p - \kappa)^2 - m_D^{*2} + i\epsilon = (m_{B_c^*}^* - \kappa_0)^2 - (\vec{\kappa}^2 + m_D^{*2}) + i\epsilon = 0,$$

$$\therefore (\kappa_0 - m_{B_c^*}^*)^2 = (\vec{\kappa}^2 + m_D^{*2}) - i\epsilon,$$

$$\begin{aligned} \kappa_0 - m_{B_c^*}^* &= \pm \sqrt{\omega_D^{*2} - i\epsilon}, \\ &= \pm \omega_D^* \mp i\epsilon, \end{aligned}$$

$$\kappa_0 = m_{B_c^*}^* - \omega_D^*. \quad (6.2)$$

The relations in Eq. (6.1) and (6.2) are used to define  $\kappa_0$  poles in the complex plane.

# Chapter 7

## Appendix B

### 7.1 SU(5) generators

Here we present the  $\lambda_i$  matrices which are the SU(5) generators in the fundamental representation of [88].

Below we explicitly show the SU(5) "Gell-Mann" matrices used, and getting the physical  $P$  and  $V$  meson matrices of Eqs. (2.10) and (2.11) respectively. The first 15 matrices are an extension of the SU(4) generators with one 0-row and one 0-column added.

$$\lambda_1 = \begin{pmatrix} 0 & 1 & 0 & 0 & 0 \\ 1 & 0 & 0 & 0 & 0 \\ 0 & 0 & 0 & 0 & 0 \\ 0 & 0 & 0 & 0 & 0 \\ 0 & 0 & 0 & 0 & 0 \end{pmatrix}, \quad \lambda_2 = \begin{pmatrix} 0 & -i & 0 & 0 & 0 \\ i & 0 & 0 & 0 & 0 \\ 0 & 0 & 0 & 0 & 0 \\ 0 & 0 & 0 & 0 & 0 \\ 0 & 0 & 0 & 0 & 0 \end{pmatrix}, \quad \lambda_3 = \begin{pmatrix} 1 & 0 & 0 & 0 & 0 \\ 0 & -1 & 0 & 0 & 0 \\ 0 & 0 & 0 & 0 & 0 \\ 0 & 0 & 0 & 0 & 0 \\ 0 & 0 & 0 & 0 & 0 \end{pmatrix},$$

$$\lambda_4 = \begin{pmatrix} 0 & 0 & 1 & 0 & 0 \\ 0 & 0 & 0 & 0 & 0 \\ 1 & 0 & 0 & 0 & 0 \\ 0 & 0 & 0 & 0 & 0 \\ 0 & 0 & 0 & 0 & 0 \end{pmatrix}, \quad \lambda_5 = \begin{pmatrix} 0 & 0 & -i & 0 & 0 \\ 0 & 0 & 0 & 0 & 0 \\ i & 0 & 0 & 0 & 0 \\ 0 & 0 & 0 & 0 & 0 \\ 0 & 0 & 0 & 0 & 0 \end{pmatrix}, \quad \lambda_6 = \begin{pmatrix} 0 & 0 & 0 & 0 & 0 \\ 0 & 0 & 1 & 0 & 0 \\ 0 & 1 & 0 & 0 & 0 \\ 0 & 0 & 0 & 0 & 0 \\ 0 & 0 & 0 & 0 & 0 \end{pmatrix},$$



$$\lambda_{22} = \begin{pmatrix} 0 & 0 & 0 & 0 & 0 \\ 0 & 0 & 0 & 0 & 0 \\ 0 & 0 & 0 & 0 & 0 \\ 0 & 0 & 0 & 0 & 1 \\ 0 & 0 & 0 & 1 & 0 \end{pmatrix}, \quad \lambda_{23} = \begin{pmatrix} 0 & 0 & 0 & 0 & 0 \\ 0 & 0 & 0 & 0 & 0 \\ 0 & 0 & 0 & 0 & 0 \\ 0 & 0 & 0 & 0 & -i \\ 0 & 0 & 0 & i & 0 \end{pmatrix}, \quad \lambda_{24} = \frac{1}{\sqrt{10}} \begin{pmatrix} 1 & 0 & 0 & 0 & 0 \\ 0 & 1 & 0 & 0 & 0 \\ 0 & 0 & 1 & 0 & 0 \\ 0 & 0 & 0 & 1 & 0 \\ 0 & 0 & 0 & 0 & -4 \end{pmatrix}.$$

## 7.2 Adjoint Representation

To obtain the matrix representations (notation) of the pseudo-scalar and the vector mesons (irreducible tensors)  $P_b^a$  and  $V_{\mu b}^a$ , we use the adjoint representation.

The matrix representation of the generator  $(T_a)_{bc}$  is given by the adjoint representation  $(\tilde{T}_a)_{bc}$ ,

$$(T_a)_{bc} = -if_{abc} \equiv [ad(T_a)]_{bc} \equiv (\tilde{T}_a)_{bc}, \quad (7.1)$$

They satisfy,  $[T_a, T_b] = if_{abc}T_c = [\tilde{T}_a, \tilde{T}_b] = if_{abc}\tilde{T}_c$ . Using the Cartesian components  $\phi$ ,

$$\phi = \begin{pmatrix} \phi_1 \\ \vdots \\ \phi_n \end{pmatrix} = (\phi)_a. \quad (7.2)$$

Then, the vector notation  $\phi_b$  in the adjoint representation, or, the  $\phi = T_b\phi_b$  transforms under the general SU(N) group transformation,

$$\begin{aligned} T_b\phi_b \rightarrow T_b\phi'_b &= T_b[\exp(-i\theta^a\tilde{T}_a)]_b^c\phi_c, \\ &\simeq T_b[1 - i\theta^a\tilde{T}_a]_b^c\phi_c, \\ &= T_b\phi_b - iT_b\theta^a(\tilde{T}_a)_b^c\phi_c, \\ &= T_b\phi_b - iT_b\theta^a(-if_{abc})\phi_c, \\ &= T_b\phi_b - iT_b\theta^a(if_{acb})\phi_c, \\ &= T_b[\phi_b - i\theta^a(if_{acb})T_b\phi_c], && (b \leftrightarrow c, \text{ next line}), \\ &= T_b\phi_b - i\theta^a(if_{abc})T_c\phi_b, \\ &= \phi - i\theta^a(if_{abc})T_c\phi_b. \end{aligned} \quad (7.3)$$

In the same way, in the matrix notation of  $\phi$  in the adjoint representation is given by,

$$(\phi)_a^b = \phi_B (T_B)_a^b = \phi^B (T_B)_a^b \quad (B = 1, 2, \dots, N). \quad (7.4)$$

In the above,  $T_B$  is the generator. We define the unitary operator  $U$  as:

$$U \equiv \exp(-i\theta^A T^A) = \exp(-i\theta^A T_A), \quad (7.5)$$

and the  $\phi$  transformations as  $\phi'$ , by changing notation as  $(A, B, C) \rightarrow (a, b, c)$ :

$$\begin{aligned} (\phi) \rightarrow \phi' &= U\phi U^\dagger, \\ &= U\phi_b T_b U^\dagger, \\ &\simeq \phi_b T_b - (i\theta^a [T_a, T_b])\phi^b, \\ &= \phi - (i\theta^a i f_{abc} T_c)\phi^b, \\ &= \phi - i\theta^a (i f_{abc}) T_c \phi^b. \end{aligned} \quad (7.6)$$

Thus, Eqs. (7.3), (7.6) with Eq. (7.4), show that the both representations are equivalent.

In this thesis, we rely on the matrix representation (notation).

# Chapter 8

## Appendix C

### 8.1 Coupling constant calculation

Developed by J.J. Sakurai in 1960s [89], the VMD model describes interactions between energetic photons and hadronic matter.

The coupling constants used in our calculation were obtained within the framework of the VMD model.

The virtual photon in the process  $e^- B^+ \rightarrow e^- B^+$  (and  $e^- B^0 \rightarrow e^- B^0$ ) is coupled to vector mesons  $\rho, \omega$ , and  $\Upsilon$ , which are then coupled to the bottom meson.

The bellow equation is valid at zero momentum transfer,

$$\sum_{V=\rho,\omega,\Upsilon} \frac{\gamma_V f_{VB^+B^+}}{m_V^2} = e. \quad (8.1)$$

Where  $\gamma_V$  is the photon-vector-meson mixing amplitude and can be determined from the vector meson partial decay width to  $e^+e^-$ , for example,

$$\Gamma_{Vee} = \frac{\alpha \gamma_V^2}{3m_V^3}. \quad (8.2)$$

Where  $\alpha$  is the fine structure constant and its value is  $\alpha = e^2/4\pi$ .

Let us consider  $f_{VBB} \equiv f_{VB^+B^+}$  and thus  $f_{\rho B^+B^+} = -f_{\rho B^+B^+}$  from isospin symmetry, we then have:

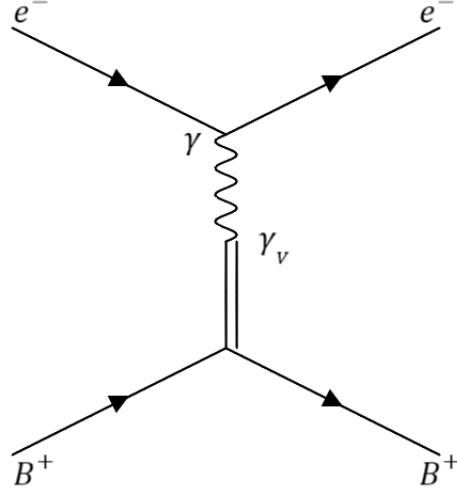


Figure 8.1: VDM feynman diagram

$$\frac{\gamma_\rho f_{\rho BB}}{m_\rho^2} = \frac{1}{2}e, \quad (8.3)$$

$$\frac{\gamma_\omega f_{\omega BB}}{m_\omega^2} = \frac{1}{6}e, \quad (8.4)$$

$$\frac{\gamma_\Upsilon f_{\Upsilon BB}}{m_\Upsilon^2} = \frac{1}{3}e. \quad (8.5)$$

We can then, write:

$$\gamma_V = m_V \sqrt{\frac{3m_V \Gamma_{Vee}}{\alpha}} \quad (8.6)$$

Using the definitions of Eq. (8.2) with  $|e| = \sqrt{4\pi\alpha}$  in the above equations:

$$\begin{aligned} f_{\Upsilon BB} &= \frac{1}{3}\alpha \sqrt{\frac{4\pi m_\Upsilon}{3\Gamma_{(\Upsilon \rightarrow e^+e^-)}}} \\ &= \frac{1}{3} \frac{1}{137.036} \sqrt{\frac{4\pi \times 9460.30 \times 10^3}{3 \times 1.340}} \\ &= \frac{1}{3}(39.683474\dots) \\ &= 13.2 \end{aligned} \quad (8.7)$$

$\Gamma_{Ve^+e^-}$  is experimental value obtained from PDG [11]. It is possible to obtain the coupling constants:

$$f_{\rho BB} = 2.48, \tag{8.8}$$

$$f_{\omega BB} = 2.84, \tag{8.9}$$

$$f_{\Upsilon BB} = 13.2. \tag{8.10}$$

Note that the value in Eq. (2.26) is the same as in Eq. (8.10).

# Bibliography

- [1] G. N. Zeminiani, S. L. P. G. Beres and K. Tsushima, “In-medium mass shift of two-flavored heavy mesons,  $B_c$ ,  $B_c^*$ ,  $B_s$ ,  $B_s^*$ ,  $D_s$  and  $D_s^*$ ,” [arXiv:2401.00250 [hep-ph]].
- [2] F. Halzen, A. D. Martin “Quarks & Leptons: An Introductory Course in Modern Particle Physics”, John Wiley & Sons, Inc, (1984).
- [3] Y. Nambu, “Quarks. Frontiers in Elementary Particle Physics,” World Scientific, 1985.
- [4] D. Griffiths, “Introduction to elementary particles,” Willey, 2008.
- [5] T. W. B. Kibble, “The Standard Model of Particle Physics,” [arXiv:1412.4094 [physics.hist-ph]].
- [6] J. Butterworth, Phil. Trans. Roy. Soc. Lond. A **374**, 20150260 (2016).
- [7] S. F. Novaes, “Standard model: An Introduction,” [arXiv:hep-ph/0001283 [hep-ph]].
- [8] D. Menezes, K. D. Marquez, T. J. N. da Silva, “Introdução a Física Nuclear e de Hadrons”, 2 ed. rev. e ampl. Sao Paulo: Livraria da Fisica (2022).
- [9] G. Yang, J. Ping and J. Segovia, Symmetry **12**, 1869 (2020).
- [10] S. L. Olsen, T. Skwarnicki and D. Zieminska, Rev. Mod. Phys. **90**, 015003 (2018).
- [11] R. L. Workman *et al.* [Particle Data Group], PTEP **2022**, 083C01 (2022).
- [12] Y. R. Liu, H. X. Chen, W. Chen, X. Liu and S. L. Zhu, Prog. Part. Nucl. Phys. **107**, 237 (2019).
- [13] H. L. Anderson, E. Fermi, E. A. Long and D. E. Nagle, Phys. Rev. **85**, 936 (1952).

- [14] Fayyazuddin and, Riazuddin “A Modern Introduction to Particle Physics, 3dr ed.” WORLD SCIENTIFIC, 2011.
- [15] K. Tsushima, “Hadron properties in nuclear medium and their impacts on observables,” [arXiv:hep-ph/0206069 [hep-ph]].
- [16] W. K. Brooks, S. Strauch and K. Tsushima, J. Phys. Conf. Ser. **299**, 012011 (2011).
- [17] R. S. Hayano and T. Hatsuda, Rev. Mod. Phys. **82**, 2949 (2010).
- [18] M. Ichikawa, T. N. Takahashi, K. Aoki, S. Ashikaga, E. Hamada, R. Honda, Y. Igarashi, M. Ikeno, D. Kawama and M. Naruki, *et al.* IEEE Trans. Nucl. Sci. **66**, 2022 (2019).
- [19] C. A. Bertulani and M. S. Hussein, Braz. J. Phys. **45**, 730 (2015).
- [20] T. Ludlam and L. McLerran, Phys. Today **56N10**, 48 (2003).
- [21] A. W. Thomas, AIP Conf. Proc. **1374**, 145 (2011).
- [22] V. Metag, M. Nanova and K. T. Brinkmann, EPJ Web Conf. **134**, 03003 (2017).
- [23] J. Hoelck and G. Wolschin, Eur. Phys. J. A **53**, 241 (2017).
- [24] J. W. Harris and B. Muller, Ann. Rev. Nucl. Part. Sci. **46**, 71 (1996).
- [25] R. Pasechnik and M. Šumbera, Universe **3**, 7 (2017).
- [26] N. R. F. Braga and L. F. Ferreira, Phys. Lett. B **783**, 186 (2018).
- [27] V. L. Eletsky, B. L. Ioffe and J. I. Kapusta, “In-medium modification of rho mesons produced in heavy ion collisions,”. [arXiv:hep-ph/9807301 [hep-ph]].
- [28] V. Metag, M. Nanova and E. Y. Paryev, Prog. Part. Nucl. Phys. **97**, 199 (2017).
- [29] J. R. Morones-Ibarra, M. Menchaca Maciel, A. Santos-Guevara and F. R. Padilla, Pramana **80**, 479 (2013).
- [30] R. Chhabra and K. Tsushima, J. Phys. Conf. Ser. **1690**, 012108 (2020).
- [31] J. P. B. C. de Melo and K. Tsushima, Phys. Lett. B **788**, 137 (2019).

- [32] T. U. Hilger, “Medium Modifications of Mesons,” Ph.D thesis, Institut für Theoretische Physik Fachrichtung Physik Fakultät Mathematik und Naturwissenschaften der Technischen Universität Dresden, Dresden (2012)
- [33] V. Metag, Prog. Part. Nucl. Phys. **61**, 245 (2008).
- [34] Menchaca-Maciel, M.C., Morones-Ibarra, J.R. Indian J Phys 87, 385 (2013).
- [35] A. J. Arifi, P. T. P. Hutauruk and K. Tsushima, Phys. Rev. D **107**, 114010 (2023).
- [36] S. Strauch *et al.* [Jefferson Lab Hall A], Fizika B **20**, 149 (2011).
- [37] G. Aad *et al.* [ATLAS], Phys. Rev. C **107**, 054912 (2023).
- [38] S. H. Lee AAPPS Bull. **31**, 3 (2021).
- [39] S. H. Lee, Symmetry **15**, 799 (2023).
- [40] K. Tsushima, PTEP **2022**, 043D02 (2022).
- [41] S. Okubo, Phys. Lett. **5**, 165 (1963).
- [42] G. Zweig, “An SU(3) model for strong interaction symmetry and its breaking. Version 2,” CERN-TH-412. (1964)
- [43] J. Iizuka, Prog. Theor. Phys. Suppl. **37**, 21 (1966).
- [44] Abe, Fumio *et al.* Physical Review D 58 (1998).
- [45] G. Krein, A. W. Thomas and K. Tsushima, Phys. Lett. B **697**, 136 (2011).
- [46] J. Cobos Martinez, K. Tsushima, G. Krein and A. W. Thomas, PoS **PANIC2021**, 199 (2022).
- [47] J. J. Cobos-Martínez, K. Tsushima, G. Krein and A. W. Thomas, Phys. Lett. B **811**, 135882 (2020).
- [48] G. Zeminiani, J. J. Cobos-Martínez and K. Tsushima, PoS **PANIC2021**, 208 (2022).
- [49] G. N. Zeminiani, Master Thesis of Universidade Cidade de São Paulo, “ $\Upsilon$  and  $\eta_b$  mass shifts in nuclear matter and the nucleus bound states,” [arXiv:2201.09158 [nucl-th]].

- [50] B. Martín-González, P. G. Ortega, D. R. Entem, F. Fernández and J. Segovia, *Phys. Rev. D* **106**, 054009 (2022).
- [51] S. S. Gershtein, V. V. Kiselev, A. K. Likhoded and A. V. Tkabladze, *Phys. Usp.* **38**, 1 (1995).
- [52] G. N. Zeminiani, J. J. Cobos-Martinez and K. Tsushima, *Eur. Phys. J. A* **57**, 259 (2021).
- [53] C. W. Liu and B. D. Wan, *Phys. Rev. D* **105**, 114015 (2022).
- [54] A. A. Karyasov, A. P. Martynenko and F. A. Martynenko, *Nucl. Phys. B* **911**, 36 (2016).
- [55] A. Tumasyan *et al.* [CMS], *Phys. Rev. Lett.* **128**, 252301 (2022).
- [56] R. Aaij *et al.* [LHCb], *Phys. Rev. Lett.* **114**, 132001 (2015).
- [57] R. Aaij *et al.* [LHCb], *Phys. Rev. D* **92**, 112002 (2015).
- [58] J. Charles, S. Descotes-Genon, Z. Ligeti, S. Monteil, M. Papucci, K. Trabelsi and L. Vale Silva, *Phys. Rev. D* **102**, 056023 (2020).
- [59] M. Artuso, E. Barberio and S. Stone, *PMC Phys. A* **3**, 3 (2009).
- [60] M. Borysova [NA60+], PoS **ICHEP2022**, 978.
- [61] R. Arnaldi [NA60+], “Prospects for open heavy-flavour and quarkonium measurements with NA60+,” [arXiv:2308.01224 [nucl-ex]].
- [62] X. J. Li, Y. S. Li, F. L. Wang and X. Liu, “Whole  $B_c$  meson spectroscopy under the unquenched picture,” [arXiv:2308.07206 [hep-ph]].
- [63] G. Alonso-Álvarez and M. Escudero, “The first limit on invisible decays of  $B_s$  mesons comes from LEP,” [arXiv:2310.13043 [hep-ph]].
- [64] H. J. Kim and H. C. Kim, “ $D_{s0}^*(2317)$  and  $B_{s0}^*$  as molecular states,” [arXiv:2310.13370 [hep-ph]].

- [65] N. Penalva, J. M. Flynn, E. Hernández and J. Nieves, “Study of new physics effects in  $\bar{B}_s \rightarrow D_s^{(*)} \tau^- \bar{\nu}_\tau$  semileptonic decays using lattice QCD form factors and heavy quark effective theory,” [arXiv:2304.00250 [hep-ph]].
- [66] M. A. K. Lodhi, F. Akram and S. Irfan, Phys. Rev. C **84**, 034901 (2011).
- [67] A. Barone, S. Hashimoto, A. Jüttner, T. Kaneko and R. Kellermann, “Approaches to inclusive semileptonic  $B_{(s)}$ -meson decays from Lattice QCD,” [arXiv:2305.14092 [hep-lat]].
- [68] P. A. M. Guichon, Phys. Lett. B **200**, 235 (1988).
- [69] K. Saito, K. Tsushima and A. W. Thomas, Prog. Part. Nucl. Phys. **58**, 1 (2007).
- [70] K. Tsushima, K. Saito, A. W. Thomas and S. V. Wright, Phys. Lett. B **429**, 239 (1998) [erratum: Phys. Lett. B **436**, 453 (1998)].
- [71] K. Tsushima, “Hadron properties in a nuclear medium and effective nuclear force from quarks: the quark-meson coupling model,” [arXiv:1912.12461 [nucl-th]].
- [72] G. Krein, J. Phys. Conf. Ser. **422**, 012012 (2013).
- [73] K. Tsushima, D. H. Lu, G. Krein and A. W. Thomas, Phys. Rev. C **83**, 065208 (2011).
- [74] J. J. Cobos-Martínez, K. Tsushima, G. Krein and A. W. Thomas, Phys. Lett. B **771**, 113 (2017).
- [75] J. J. Cobos-Martínez, K. Tsushima, G. Krein and A. W. Thomas, Phys. Rev. C **96**, 035201 (2017).
- [76] J. J. Cobos-Martínez, K. Tsushima, G. Krein and A. W. Thomas, J. Phys. Conf. Ser. **912**, 012009 (2017).
- [77] J. J. Cobos-Martínez, K. Tsushima, G. Krein and A. W. Thomas, PoS **Hadron2017**, 209 (2018).
- [78] K. Tsushima, D. H. Lu, G. Krein and A. W. Thomas, AIP Conf. Proc. **1354**, 39 (2011).

- [79] G. Krein, A. W. Thomas and K. Tsushima, *Prog. Part. Nucl. Phys.* **100**, 161 (2018).
- [80] J. R. Stone, P. A. M. Guichon, P. G. Reinhard and A. W. Thomas, *Phys. Rev. Lett.* **116**, 092501 (2016).
- [81] P. A. M. Guichon, J. R. Stone and A. W. Thomas, *Prog. Part. Nucl. Phys.* **100**, 262 (2018).
- [82] Z. w. Lin and C. M. Ko, *Phys. Lett. B* **503**, 104 (2001).
- [83] F. Akram, Ph.D thesis, Physics Department University of the Punjab Lahore, Pakistan (2013).
- [84] K. Huang, *Int. J. Mod. Phys. A* **28**, 1330050 (2013).
- [85] G. 't Hooft and M. J. G. Veltman, *Nucl. Phys. B* **44**, 189 (1972).
- [86] C. G. Bollini and J. J. Giambiagi, *Nuovo Cim. B* **12**, 20 (1972).
- [87] G. M. Cicutta and E. Montaldi, *Lett. Nuovo Cim.* **4**, 329 (1972).
- [88] F. Stancu, *Few Body Syst.* **64**, 60 (2023).
- [89] J. J. Sakurai, *Annals Phys.* **11**, 1 (1960)